Genome-wide fitness assessment during diurnal growth reveals an expanded role of the cyanobacterial circadian clock protein KaiA

David G. Welkie[1], Benjamin E. Rubin[2], Yong-Gang Chang[3], Spencer Diamond[2,4], Scott A. Rifkin[2], Andy LiWang[3], Susan S. Golden[1,2]

[1]Center for Circadian Biology, University of California, San Diego, La Jolla, CA; [2]Division of Biological Sciences, University of California San Diego, La Jolla CA; [3]School of Natural Sciences, University of California, Merced, CA; [4]Department of Earth and Planetary Science, University of California, Berkeley, CA.

Abstract

The recurrent pattern of light and darkness generated by Earth's axial rotation has profoundly influenced the evolution of organisms, selecting for both biological mechanisms that respond acutely to environmental changes and circadian clocks that program physiology in anticipation of daily variations. The necessity to integrate environmental responsiveness and circadian programming is exemplified in photosynthetic organisms such as cyanobacteria, which depend on light-driven photochemical processes. The cyanobacterium *Synechococcus elongatus* PCC 7942 is an excellent model system for dissecting these entwined mechanisms. Its core circadian oscillator, consisting of three proteins KaiA, KaiB, and KaiC, transmits time-of-day signals to clock-output proteins, which reciprocally regulate global transcription. Research performed under constant light facilitates analysis of intrinsic cycles separately from direct environmental responses, but does not provide insight into how these regulatory systems are integrated during light-dark cycles. Thus, we sought to identify genes that are specifically necessary in a day-night environment. We screened a dense bar-coded transposon library in both continuous light and daily cycling conditions and compared the fitness consequences of loss of each nonessential gene in the genome. Although the clock itself is not essential for viability in light-dark cycles, the most detrimental mutations revealed by the screen were those that disrupt KaiA. The screen broadened our understanding of light-dark survival in photosynthetic organisms, identified unforeseen clock-protein interaction dynamics, and reinforced the role of the clock as a negative regulator of a night-time metabolic program that is essential for *S. elongatus* to survive in the dark.

Significance

Understanding how photosynthetic bacteria respond to and anticipate natural light–dark cycles is necessary for predictive modeling, bioengineering, and elucidating metabolic strategies for diurnal growth. Here, we identify the genetic components that are important specifically under light-dark cycling conditions and determine how a properly functioning circadian clock prepares metabolism for darkness, a starvation period for photoautotrophs. This study establishes that the core circadian clock protein KaiA is necessary to enable rhythmic de-repression of a night-time circadian program.

Specific Contributions

DGW BR SD and SSG conceived and designed the project. DGW BR and YGC performed the experiments and analyzed the data. SAR wrote the R scripts for RB-TnSeq conditional fitness analysis. YGC and AL interpreted fluorescence anisotropy data. DGW BR SSG YGC and AL wrote the manuscript.

\body

Introduction

Photosynthetic organisms experience a dramatic change in physiology and metabolism each day when the sun sets and the daytime processes related to photosynthesis become inoperative. Like many diverse organisms throughout nature, prokaryotic cyanobacteria have evolved circadian clocks that aid in the temporal orchestration of activities that are day- or night-appropriate. The circadian clock's contribution towards fitness in changing environments was first demonstrated in 1998, when it was shown that strains of the cyanobacterium *Synechococcus elongatus* PCC 7942 with intrinsic circadian periods that match that of external light-dark cycles (LDC) outcompete strains that have different periods (1, 2). More recent experiments showed the value of preparing for night: when cells synchronized to different phases of the circadian cycle are mixed and then exposed to a pulse of darkness, those whose internal clock corresponds to a dawn or day-time phase have a higher occurrence of arrested growth upon re-illumination than those synchronized to anticipate darkness at the time of the pulse (3). These data support the hypothesis that the clock acts to prepare the cell for conditions that are predictable and recurrent, such as night following day.

A fitness advantage of appropriate circadian timing signals is not exclusive to cyanobacteria, as is observed in the model plant *Arabidopsis* (4, 5) and in humans, where circadian disruption can result in myriad adverse health effects including cardiovascular disease, cancer, and sleep disorders (6–8). Although the fundamental properties of circadian rhythms are shared across the domains of life, the molecular networks that generate them vary (9). In *S. elongatus* a three-protein oscillator comprising the proteins KaiA, KaiB, and KaiC sets up a circadian cycle of KaiC phosphorylation. This oscillator even functions *in vitro* when mixed at appropriate ratios with ATP (10), which has provided a powerful tool for exploring the mechanism that generates circadian rhythms. Genetic, biochemical, metabolic, and structural inquiries have revealed that the *S. elongatus* oscillator actively turns off a night-time metabolic program prior to dawn by triggering the dephosphorylation of the master transcription factor Regulator of Phycobilisome Association A (RpaA). It accomplishes this task by recruiting Circadian Input Kinase A (CikA) to a ring of KaiB that forms on KaiC during the night-time portion of the cycle, thus activating CikA phosphatase activity against RpaA (11–13). Among the targets of the RpaA regulon are the genes that facilitate catabolism of glycogen and generation of NADPH via the oxidative pentose phosphate pathway (14). These enzymatic reactions are essential for the cyanobacterium to survive the night when photosynthetic generation of reductant is disabled (15, 16).

While the molecular mechanisms of the circadian clock are well established in constant light for *S. elongatus* (17), its role in response to LDC, and the mechanisms by which the cell integrates circadian and environmental data, are still not understood. There have been few publications on the topic, and this study is the first to report on a genome-wide screen for LDC-sensitive mutants. Studies that report conditional LDC effects have been limited to a small number of genes. For instance, mutants defective for the circadian clock output pathway genes, *rpaA* and *sasA* (15, 16, 18, 19), and mutants unable to mobilize carbon through the oxidative pentose phosphate pathway (OPPP) and glycogen breakdown (16, 20, 21), or unable to synthesize the alarmone nucleotide ppGpp (22, 23), have conditional defects specific to growth in LDC. To identify the genetic contributors to fitness under LDC and acquire a more comprehensive picture of the regulatory network, we used an unbiased population-based screen that tracks the fitness contributions of individual *S. elongatus* genes to reproduction in diel cycles. The method, random bar code transposon-site sequencing (RB-TnSeq), quantitatively compares the changes in abundances of individuals in a pooled mutant population over time. This assay allowed the calculation of a fitness contribution to LDC survival for each nonessential gene in the genome by leveraging multiple inactivating mutations spread across a genomic locus. This library was previously used to identify the essential gene set of *S. elongatus* under standard laboratory

continuous light conditions (CLC) (24) and to generate an improved the metabolic model for generating phenotype predictions (25).

The results described here provide a comprehensive picture of genes that contribute to fitness under diurnal growth conditions. In addition to identifying the genetic components previously known to be critical for growth in LDC we found ~100 new genes whose mutation confers weak to strong fitness disadvantages. Of these genes, we focused on the top-scoring elements for LDC-specific defects which, unexpectedly, lie within the *kaiA* gene of the core circadian oscillator. As no previously known roles for KaiA predicted this outcome, we characterized the mechanism that underlies the LDC sensitivity of a *kaiA*-null mutant, and revealed interactions within the oscillator complex that regulate the activation of CikA, an RpaA phosphatase.

Results

Growth of library mutants to assess genetic fitness contributions under light-dark cycles.

The RB-TnSeq mutant library includes a unique identifier sequence, or bar code, at each insertion site to track each transposon-insertion mutant. Next-generation sequencing is used to quantify these bar codes within the total DNA of the population, such that the survival and relative fitness of the approximately 150,000 mutants in the library can be tracked under control and experimental conditions (26). In this way, the *S. elongatus* RB-TnSeq library can be used for pooled, quantitative, whole-genome mutant screens.

First, the library was thawed, placed into 250-mL flasks, and sampled during incubation in CLC under only the selective pressure for the transposon antibiotic-resistance marker. Genomic DNA was extracted, and the bar codes of the mutant population were sequenced to establish a baseline abundance (**Fig. 1**). The culture was then divided into photobioreactors set to maintain constant optical density under either CLC, or LDC conditions that mimic day and night. After a treatment period allowing for approximately 6 generations, the library was again sampled and bar codes were quantified in a similar fashion. By comparing the frequencies of the bar codes after growth in LDC to those in CLC (**Dataset S1**), we estimated a quantitative measure of the fitness contribution for each gene specifically under LDC (**Dataset S2**).

After filtering the data as described in the Materials and Methods section we were able to analyze insertions in 1,872 of the 2,005 non-essential genes (24) in the genome. Each fitness score that passed our statistical threshold for confidence (FDR <1%) was classified as having a "strong" (>1.0 or <-1.0), "moderate" (between 1.0 and 0.5 or -1.0 and -0.5) , or "negligible / minor" (between 0 and ±0.5) effect on fitness in LDC. This analysis revealed 90 loci whose disruption caused strong changes to LDC fitness (41 negatively and 49 positively) and an additional 130 loci that had moderate effects (**Fig. 2*A***). A volcano plot showing the data with selected genes highlighted in this study is displayed in **Fig. 2*B***. Because our initial goal was to understand the suite of genes required to survive the night, we focused first on those mutants whose loss specifically debilitates growth in LDC.

Metabolic pathways important for LDC growth

The functional composition of genes found to be either detrimental or favorable to fitness is indicative of the metabolic processes that are important for growth in LDC (**Fig. 2*C***). Genes identified as necessary in LDC encode enzymes that participate in carbohydrate and central carbon metabolism, protein turnover and chaperones, CO_2 fixation, and membrane biogenesis. Strikingly, all genes of the OPPP, *zwf*, *opcA*, *pgl*, and *gnd,* have strong fitness effects (**Fig. 3*A***). In addition, *tal*, the only non-essential gene of the reductive phase, is also essential for LDC growth. It is known that *tal* mRNA peaks at dusk and that its product acts in a reaction that is shared between the oxidative and reductive phases of the PPP, linking it to glycolysis; the *tal* mutant's sensitivity to LDC supports the hypothesis that Tal is a less recognized, but important,

component of the OPPP reactions. Furthermore, all OPPP genes have peak expression at dusk (27).

Disruptions in genes that encode enzymes responsible for glycogen metabolism previously have been shown to cause LDC sensitivity (21). Our screen clearly identified the genes for catabolic glycogen metabolism *glgX* and *glgP* as important LDC fitness factors (**Fig. 2*B***). However, the importance of glycogen metabolism in LDC fitness is complicated by evidence that the anabolic reactions of *glgA* and *glgC* contribute to fitness in CLC as well, due to the utilization of glycogen as a sink for excess photosynthetically derived electrons (28, 29). Thus, for genes critical for glycogen anabolism, the differential LDC fitness score is not as striking as might be expected from phenotypic assays of those mutants. The *glgA* mutants were classified as having a minor LDC defect, and insufficient reads for *glgC* removed this locus from our analysis pipeline, leading to a classification of "not determined". Despite this complication, mutations in the gene *glgB,* whose product catalyzes the last non-essential step in glycogen synthesis, caused a strong decrease in LDC fitness, supporting the conclusion that both glycogen synthesis and breakdown are critical aspects of metabolism in LDC conditions. Together, the reactions facilitated by these enzymes provide a major source of reductant (NADPH) in the dark and facilitate the flow of glucose compounds via the breakdown of stored glycogen into downstream metabolites.

Genes involved in DNA repair (such as the transcription-repair coupling factor *mdf*) and chaperone systems (*clpB1*) are also important for light-dark growth. ClpB1 is known to contribute to thermotolerance stress and is induced upon dark-light transitions in cyanobacteria (30, 31). The importance of these genes for surviving light-dark cycles suggests a role in managing light-induced stress that the transition from dark to light may impose. Moreover, mutation of any of the three genes that encode enzymes of the glycine cleavage system confer increased LDC fitness. The glycine decarboxylase complex (GDC) is linked to photorespiratory mechanisms that respond to high-light stress (32, 33). This result further supports our finding that variations in the fitness of metabolism genes between CLC and LDC are linked to pathways that mitigate light stress.

In addition to underscoring the importance of the OPPP, glycogen metabolism, and repair mechanisms in LDC, we also found a strong link between these metabolic pathways and circadian clock management. Many of the genes essential for growth in LDC are regulated by the clock output protein RpaA. For instance, the circadian clock gene *kaiC* is itself regulated by RpaA and its expression is reduced by over 50% in an *rpaA*-null background (12, 14). This attribute is also shared by the core glycogen metabolism and PPP genes *glgP*, *zwf*, *opcA*, *gnd*, and *tal,* and genes involved with metal ion homeostasis (*smtA*) and cobalamin biosynthesis (*cobL*), all of which show significantly reduced transcripts (<-1.0 log2(*ΔrpaA*/WT, wild type) in the absence of the RpaA (14). These core glycogen metabolism and PPP genes , with the exception of *tal* and *gnd,* are also direct targets of the transcription factor. This finding is a common trend in mutants that show strong fitness decreases in LDC, as ~20% (9/41) have dramatic reductions in mRNA levels in an *rpaA*-null strain. This trend is not the case for any of the genes identified as mutants that confer increased fitness (**Fig 3*B***). These findings support a growing body of evidence that the ability of *S. elongatus* to initiate a night-time transcriptional program, and particularly to activate the OPPP pathway genes, is critical for survival through darkness (15, 16).

Fitness contributions of circadian clock constituents

The mechanism of circadian timekeeping and regulation in cyanobacteria is well understood at the molecular level (17, 34). The three core clock proteins, KaiA, KaiB, and KaiC orchestrate circadian oscillation in *S. elongatus* (35), whereby KaiC undergoes a daily rhythm of

189 phosphorylation and dephosphorylation that provides a time indicator to the cell (36, 37). During
190 the day period, KaiA stimulates KaiC autophosphorylation, and, during the night, KaiB opposes
191 KaiA's stimulatory activity by sequestering an inactive form of KaiA (38), leading to KaiC
192 autodephosphorylation. Two histidine kinase proteins, SasA and CikA, engage with the
193 oscillator at different phases of the cycle, and this interaction stimulates SasA kinase activity to
194 phosphorylate RpaA and later stimulates CikA phosphatase activity to dephosphorylate RpaA.
195 Thus, phosphorylated RpaA accumulates during the day, peaking at the day-night transition,
196 and activates the night-time circadian program.

197 Mutations that caused the most serious defect specifically in LDC were mapped to the gene that
198 encodes the clock oscillator component KaiA (**Fig. 2*B***). This outcome was unexpected because
199 the known roles of KaiA are to stimulate phosphorylation of KaiC and to enable normal levels of
200 KaiC and KaiB expression (38, 39). Thus, a KaiA-less strain, in which KaiC levels are low and
201 hypophosphorylated (39), was expected to behave like a *kaiC* null. A *kaiC* null mutant has no
202 notable defect in LDC when grown in pure culture (1), and even a *kaiABC* triple deletion,
203 missing KaiA as well as KaiB and KaiC, grows well in LDC (18).

204 Nonetheless, a *kaiC* null mutant is known to be outcompeted by WT under LDC conditions in
205 mixed culture (1, 2), which is the situation in this population-based screen. Mutations in *kaiC*
206 returned negative fitness scores in the current screen, as did bar codes associated with *rpaA*
207 and *sasA*, two clock-related genes that are known to be important for growth in LDC (18, 20).
208 RpaA is important for redox balancing, metabolic stability, and carbon partitioning during the
209 night, and an *rpaA* mutant is severely impaired in LDC (15, 16, 20). While it is identified in the
210 current screen as LDC sensitive, inactivation of *rpaA* also confers a moderate fitness decrease
211 under CLC (~-1.0), thus diminishing the differential LDC-specific fitness calculation.

212 Disruptions to other genes related to circadian clock output scored as beneficial to growth in
213 LDC, increasing the fitness of the strains against the members of the population that carry an
214 unmutated copy. For instance, mutations within the gene that encodes CikA showed improved
215 fitness, along with disruptions to the sigma factor encoded by *rpoD2* (40). CikA has several
216 roles that affect the clock, including synchronization with the environment and maintenance of
217 WT period; additionally, CikA is stimulated to dephosphorylate RpaA by association with the
218 oscillator at night (13, 41). Thus, a phenotype for *cikA* mutants that is opposite to that of *sasA*
219 mutants forms a consistent pattern.

220 From the published biochemical data we would predict that, in a *kaiA* null, SasA kinase would
221 still be activated by the low levels of unphosphorylated KaiC but that CikA phosphatase would
222 not be: CikA binds not to KaiC, but to a ring of KaiB that engages hyperphosophorylated KaiC, a
223 state that is not achieved in the absence of KaiA. Therefore, we would expect that RpaA would
224 be constitutively phosphorylated in a *kaiA* null mutant and that the cell would be fixed in the
225 night-time program, where it would be insensitive to LDC. We further investigated the *kaiA*-
226 mutant phenotype under LDC to test the validity of the RB-TnSeq results.

227 ***Growth attenuation and rescue of a kaiA mutant.*** The strong negative scores of bar codes
228 for *kaiA* insertion mutants pointed to a severe growth defect in LDC. In order to vet this finding
229 we tested the phenotype of an insertional knockout of the *kaiA* gene (*kaiA*^{ins}), similar to the
230 strains in the RB-TnSeq library. Assays in CLC vs LDC verified the LDC-specific defect in the
231 mutant (**Fig. 4*A***). Because *kaiABC* deletion mutants and *kaiC* deletion mutants both do not
232 have an LDC defect in pure culture, the LDC defect seemed to be specific for situations in which
233 KaiC and KaiB are present without KaiA. The *kaiA* coding region has a known negative element
234 located within its C-terminal coding region that negatively regulates expression of the
235 downstream *kaiBC* operon (42, 43) (*kaiA*^{ins}), keeping KaiBC levels low. We reasoned that the
236 loss of KaiA would be exacerbated if expression of KaiBC increased. To test this hypothesis, we

measured the growth characteristics of a *kaiA* mutant in which the coding region of *kaiA*, including the negative element, has been removed and replaced with a drug marker (*kaiA*^{del}) (39). This strain, which is known to have normal or slightly elevated levels of KaiB and KaiC, exhibited even more dramatic sensitivity to LDC and supported the hypothesis that an unbalanced clock output signal underlies the LDC sensitivity in the *kaiA* mutant.

Knowing that *rpaA*-null mutants, which cannot activate the OPPP genes, have similarly severe LDC phenotypes, we hypothesized that the *kaiA*-less strains have insufficient phosphorylation of RpaA to turn on those genes. We reasoned that additionally interrupting the *cikA* gene, whose product dephosphorylates RpaA in a clock-dependent manner, would help to conserve RpaA phosphorylation in the *kaiA*^{del} strain and increase LDC fitness. Indeed, mutations that disrupt *cikA* were identified from the population screen as enhancing fitness (**Fig. 2*B*),** a finding we confirmed in a head-to-head competitive growth assay in a mixed culture with WT (**Fig. 4*B***). Complementation of this double mutant with a *cikA*^{WT} gene, or the *kaiA*^{del} strain with *kaiA*^{WT} expressed from a neutral site in the genome, resulted in a reversal of the respective phenotypes (**Fig. S1**). The LDC growth defects in *kaiA*^{del} and improvement of the *kaiA*^{del}*cikA* strain were reproducible when grown in liquid cultures in the same photobioreactors used to grow the library for the LDC screen (**Fig. 4*C***). These results are consistent with a model in which, in the absence of KaiA, CikA is constitutively activated as a phosphatase to dephosphorylate RpaA.

Arrhythmic and low* kaiBC *expression correlates with LDC phenotype. Hallmarks of RpaA deficiency or dephosphorylation are low and arrhythmic expression from the *kaiBC* locus under CLC, as visualized using a luciferase-based reporter (P_{kaiBC}*::luc*) (12). We used this assay to determine whether the severity of defect in LDC growth in mutants correlates with level of expression from this promoter as a proxy for RpaA phosphorylation levels. Consistent with the hypothesis, the *kaiA*^{ins} mutant has low constitutive levels of luciferase activity, tracking near the troughs of WT circadian expression, the *kaiA* deletion mutant has almost undetectable expression, and the constitutive expression from the *kaiABC*^{del} strain tracks near peak WT levels (**Fig. 5**). Moreover, the *kaiA*^{del}*cikA* strain shows expression levels much higher than the *kaiA*^{del} strain, approaching those observed in the *kaiABC*^{del} mutant and around the midline of WT oscillation. Intermediate levels of growth in LDC between the *kaiA*^{del} and *kaiA*^{del}*cikA* strains were observed when a *cikA* variant (C644R) that is predicted to have reduced KaiB binding, and thus less phosphatase activation, was expressed in *trans* in the *kaiA*^{del}*cikA* strain (11). Growth of this strain also displayed intermediate LDC sensitivity (**Fig. 4*A*)**. These data support a correlation between expression from the P_{kaiBC}*::luc* reporter strain, likely reflecting RpaA phosphorylation levels, and growth in LDC.

Low RpaA phosphorylation in* kaiA*-null cells as the cause of decreased fitness. We next directly assayed the RpaA phosphorylation levels in this group of mutants by using immunoblots and Phos-tag reagent to separate phosphorylated (P-RpaA) from unphosphorylated RpaA. As predicted, P-RpaA was low in the *kaiA*^{ins} mutant and almost undetectable in the *kaiA*^{del} strain (**Fig. 6*A***). Adding an ectopic WT *kaiA* allele, or disrupting *cikA*, in the *kaiA*^{del} mutant restored RpaA phosphorylation. Thus, even though adequate KaiC is present to engage SasA to phosphorylate RpaA (**Fig. 5*B*)**, the absence of KaiA is sufficient to suppress RpaA phosphorylation. These results support the conclusion that the rescue of the *kaiA* growth defect by disrupting *cikA* is due to the elimination of CikA phosphatase activity.

Because the model suggests that turning on RpaA-dependent genes at dusk is critical for survival in LDC, we measured P-RpaA specifically at light-to-dark and dark-to-light transitions in *kaiA*^{del} and *kaiA*^{del}*cikA* over three diel cycles. WT has a marked pattern of high P-RpaA at dusk and low levels at dawn (**Fig. 6*C***). The *kaiA*^{del} strain had almost undetectable levels of P-RpaA, visible only when the overall RpaA signal was very high. The P-RpaA phosphorylation status in

285 the *kaiA*^{del}*cikA* was restored but did not show diel variations, consistent with the arrhythmicity of
286 *kaiA* mutants.

287 Other physiological similarities between the *kaiA*-null and *rpaA*-null strains exist. An *rpaA*
288 mutant accumulates excessive reactive oxygen species (ROS) during the day that it is unable to
289 alleviate during the night (15). Metabolomic analysis points towards a deficiency in reductant,
290 needed to power detoxification reactions for photosynthetically-generated ROS, due to lack of
291 NADPH production in the dark when OPPP genes are not activated. Likewise, levels of ROS in
292 *kaiA*^{del} were significantly higher at night than in WT and *kaiA*^{del}*cikA* (**Fig. 6*D***).

293 ***Molecular basis of CikA engagement in the absence of KaiA***. The proposal that the LDC
294 fitness defects in *kaiA* mutants result from excessive CikA phosphatase activity was derived
295 from genetic data related to known LDC-defective mutants. However, previous studies
296 regarding KaiA activities had not predicted this outcome. Very recent structural data, enabled
297 through the assembly of KaiABC and KaiBC-CikA complexes, pointed to a likely mechanism:
298 loss of competition for a binding site on KaiB that KaiA and CikA share (11). Although this
299 hypothesis was appealing, the current model of progression of the Kai oscillator cycle could not
300 predict this outcome. KaiA and CikA bind to a ring of KaiB that forms after KaiC has become
301 phosphorylated at Serine 431 and Threonine 432 (44). Maturation to this state induces
302 intramolecular changes in KaiC that expose the KaiB binding site. In the absence of KaiA, KaiC
303 autophosphorylation is extremely abated as measured both *in vivo* (45) and *in vitro* (1-10%, **Fig.
304 S5C**), so how can KaiB bind?

305 We used fluorescence anisotropy to directly determine whether KaiB can engage with KaiC in
306 the absence of KaiA, when KaiC is mainly unphosphorylated (**Fig. 7** and **Fig. S5**). If KaiC-KaiB
307 binding can occur, it could support binding of CikA – expected to be a necessary event for CikA
308 phosphatase activation. This method measures the magnitude of polarization of fluorescence
309 from KaiB tagged with a fluorophore (6-iodoacetamidofluorescein), which increases when KaiB
310 becomes part of a larger complex. KaiC phosphomimetic mutants were used to quantify
311 interaction of KaiB with each of the phosphostates of KaiC. Initially, we hypothesized that the
312 KaiB binding site might become exposed on KaiC in the absence of phosphorylation when cells
313 enter the dark and the ATP/ADP ratio is altered (46). For this reason, experiments were
314 performed at different ATP/ADP ratios. As a control, we confirmed that no significant association
315 of KaiB with CikA occurs in the absence of KaiC (**Fig. 7*A***). However, KaiB is able to associate
316 with hypophosphorylated WT KaiC approximately as well as with the phosphomimetic, KaiC-EA,
317 which mimics a form of KaiC (KaiC-pST) that binds KaiB, which then forms a new ring on the N-
318 terminal face of KaiC that captures KaiA and CikA. This binding was similar in both 1 mM ATP
319 and 0.5 mM ATP+0.5 mM ADP conditions (**Fig. 7*B***), suggesting that darkness (associated with
320 decreased ATP/ADP *in vivo*) is not required to enable KaiB binding to KaiC. Moreover, CikA
321 associated with KaiBC under both conditions. Association of KaiB was minimal with KaiC-AE, a
322 mimic of the daytime state (KaiC-SpT) when KaiA is usually well-associated with the A-loops of
323 KaiC in an interaction that does not require KaiB. However, the presence of CikA enhanced the
324 binding of KaiB to KaiC-AE, presumably due to formation of a KaiC-KaiB-CikA complex. For the
325 WT KaiC experiments in **Fig. 7**, KaiB (0.05 μM) is most likely binding to the small percentage (1-
326 10%) of the KaiC population that remains phosphorylated (0.04-0.4 μM). *In vivo*, it is likely that
327 in the absence of KaiA, KaiB also binds selectively to a phosphorylated fraction of the
328 hypophosphorylated KaiC pool.

329 These data generally match the patterns expected for the current oscillator model; however,
330 they also demonstrate that the KaiC-KaiB-CikA complex can form in the absence of KaiA, when
331 the KaiC pool is hypophosphorylated, and that the ATP ratio (mimicking day and night) has little
332 effect on this association. Furthermore, they support the competitive binding of KaiA and CikA to
333 the KaiB ring. These observations are consistent with the proposal that the low survival rate of

kaiA-null mutants is due to over-stimulation of CikA phosphatase activity, stripping the cell of P-RpaA and disabling expression of the critical night-time reductant-producing OPPP.

Discussion

Recent research and interest in growth of cyanobacteria in LDC conditions (15, 16, 20, 22, 47–49) provides a rich dataset to inform engineering strategies, to model metabolic flux predictions, and to elucidate the intersection of the clock and cell physiology. While previous studies have identified a handful of genes important for growth in LDC, the conditional defect of these mutants was determined from targeted studies that left large unknowns in the pathways important for LDC. This study used an unbiased quantitative method to comprehensively query the *S. elongatus* genome for the full set of genes that are specifically necessary to survive the night. This approach eliminated the requirement to test individual mutants for a scorable phenotype under diel conditions and allowed for the discovery of genes that would not be predicted to have such a phenotype. In addition to identifying genes of pathways previously unknown to be involved in LDC, this screen also strongly reinforced two emerging stories from recent research: the breakdown of glycogen and flux through the OPPP, the major source of reductant under non-photosynthetic conditions, is essential (15, 16); and, the role of the clock is repressive, rather than enabling (12), as its complete elimination has little consequence in LDC, but its constitutive output signaling is harmful under these conditions because of its negative effect on the OPPP genes.

A boon of the Rb-TnSeq data is in how it reveals non-intuitive insights into the regulatory measures cells need for growth in specific conditions. One such discovery is that a *kaiA* mutant is severely LDC sensitive. Investigation of the mechanism that underlies this phenotype led to increased understanding of the function of the Kai oscillator, a nanomachine whose structural interactions have been revealed with an unusual degree of clarity (11, 50). KaiA is conventionally thought to have a specific daytime role in stimulating KaiC autophosphorylation – an activity that promotes SasA stimulation and brings about the conformational change in KaiC that enables KaiB engagement (**Fig. 8*A***). This latter step ushers in the KaiC dephosphorylation phase, during which KaiA is a passive, inactive player. Results from this study provide a new perspective of KaiA in its KaiB-bound form as regulating the night-time clock output by its competition with CikA for KaiB-binding (**Fig. 8*B***). A cell without KaiA leaves the major transcription factor RpaA hypophosphorylated for two reasons. First, without KaiC undergoing its daytime phosphorylation cycle, SasA engagement with the oscillator is diminished, reducing its kinase activity acting on RpaA. Secondly, without KaiA present as a competitor, the opportunities for CikA binding on KaiB-KaiC complexes increase, leading to hyperactive phosphatase activity and ultimately eliminating any chance for phosphorylated RpaA to accumulate. The result is a severe decrease in fitness in LDC. However, cells without KaiA and CikA (and even without KaiABC) have ample P-RpaA, indicating that other pathways contribute to the phosphorylation of RpaA. This fact emphasizes the counterintuitive point that activation of CikA phosphatase in the night-time complex, rather than activation of SasA kinase, is the key signaling state of the cyanobacterial clock (12).

The screen revealed expected mutants as well. Although a *kaiC* mutant does not have a notable LDC defect in pure culture, it is known to do poorly in LDC when grown in a population with other cells that have a functioning circadian rhythm, as is the case in the pooled growth scenario used here, illustrating soft selection for circadian rhythms in cyanobacteria (1). As expected, *kaiC* scored as deficient in LDC, but not as severely as many other mutants. One of the most severely LDC-defective mutants we know of is *rpaA*, which dies within a few hours of dark exposure and requires special handling in the lab. Strains with disruptions in *rpaA* did score as negative, but only to a moderate degree (-0.7). This discrepancy between severe known phenotype and moderate score can be attributed to the fact that *rpaA* mutants were also less fit

383 than the population in CLC, decreasing its magnitude of relative fitness in LDC, similar to the
384 situation for mutants defective in glycogen anabolic processes.

385 Importantly, the screen also identified an equivalent list of genes whose loss improves growth in
386 LDC. Although not the target of the current study, these genes have great potential for providing
387 new insights into *S. elongatus* diurnal physiology and perhaps improved genetic backgrounds
388 for metabolic engineering. In contrast to many of the mutants that negatively affect LDC growth,
389 the list of top positive mutants includes many genes with less transparent roles in LDC
390 conditions, including some that carry no functional annotation. The phenotype may be
391 attributable to a specific pathway or may result from the additive effects of many unrelated
392 genes whose expression is altered in a regulon indirectly. Some mutants may outcompete
393 others in the population because they have alleviated photochemical intermediate buildup or
394 lessened the uptake of harmful metabolites in the medium. The scant information available
395 regarding these pathways makes it difficult to predict why their value would be different in CLC
396 vs. LDC.

397 In summary, this study has improved our understanding of the mechanism of core oscillator
398 protein interactions and generated a comprehensive map of genetic pathways needed for
399 survival in LDC in *S. elongatus*. We have shown that KaiA, originally thought to only regulate
400 KaiC autophosphorylation, also modulates CikA-mediated clock output. More broadly, the use of
401 RB-TnSeq on a dense transposon library in this study has identified the genes in the genome
402 necessary for growth in alternating light-dark conditions, established a firm connection between
403 circadian clock regulation and the metabolic pathways critical for fitness in more natural
404 environments, and contributed to a more complete picture of the finely balanced mechanisms
405 that underlie circadian clock output.

406

407 **Materials and Methods**

408 ***Bacterial strains and culture conditions***. All cultures were constructed using WT *S. elongatus*
409 PCC 7942 stored in our laboratory as AMC06. Cultures (**Table S1**) were grown at 30 °C using
410 either BG-11 liquid or solid medium with antibiotics as needed for selection at standard
411 concentrations: 20 µg/mL for kanamycin (Km) and gentamicin (Gm), 22 µg/mL for
412 chloramphenicol (Cm), and 10 µg/mL each for spectinomycin and streptomycin (SpSm) (51).
413 Liquid cultures were either cultivated in 100 mL volumes in 250 mL flasks shaken at ~150 rpm
414 on an orbital shaker or in 400 mL volume in top-lit bioreactors (Phenometrics Inc. ePBR
415 photobioreactors version 1.1) mixed via filtered ambient-air bubble agitation with a flow rate of
416 0.1 mL per min at 30 °C. Viable cell plating for LDC-sensitivity testing and quantification of
417 cellular ROS were performed as previously described (15). Spot-plate growth was quantified by
418 converting the plate image to 8-bit and performing densitometric analyses using National
419 Institutes of Health ImageJ software (52). Transformation was performed following standard
420 protocols (53). Strains were checked periodically for contamination using BG-11 Omni plates
421 (BG-11 supplemented with 0.04% glucose and 5% LB) (53). Verification of the disruption of the
422 *kaiA* gene in mutants was performed by PCR and is shown in **Fig. S1**. For immunoblotting
423 experiments and ROS measurements cultures were grown in flasks. Samples for protein were
424 taken after 3 light-dark cycles at specified time points immediately before the lights turned on
425 and turned off.

426 **One-on-one competition experiments**. The relative fitness of *cikA* null and *cikA*+ strains was
427 assessed in growth competition experiments that leveraged different antibiotic resistance
428 markers in the strains. The *cikA* mutant carries a Gm-resistance marker inserted in the *cikA*
429 locus. AMC06 was transformed with pAM1579 to generate a Km-resistant strain that carries the

430 drug cassette in neutral site II (designated as "WT-Km^R" for this experiment). The axenic
431 cultures were grown to OD_{750} ~ 0.4, washed three times with BG-11 via centrifugation at 4,696
432 G for 10 min to remove antibiotics, and diluted with BG-11 to an OD_{750} of 0.015. Cultures were
433 then mixed in a 1:1 ratio and grown without antibiotics for 8 days under ~100 µmol photos· m^2
434 · s^{-1} light. To assay survival of each genotype at 0, 3, and 8 days, mixed cultures were diluted
435 using a 1:10 dilution series and plated in 20 µL spots in duplicate onto ~2 mL of BG-11 agar
436 with either Gm or Km poured in the wells of a 24-well microplate. CFU's of each strain were
437 calculated from the dilution series across the two antibiotic regimes and were used to determine
438 the percentage of each strain in the mixture population over time. To ensure that the expression
439 of the antibiotic markers did not influence fitness, WT cultures that carried each drug-resistance
440 marker (Km in neutral site II via plasmid pAM1579 or Gm in neutral site III via plasmid
441 pAM5328) were grown together and assayed, and displayed no significant differences (**Fig. S2).**

442 ***Rb-Tnseq Assay.*** Samples of the library archived at -80 C were quickly thawed in a 37 C water
443 bath for 2 min and then divided into three flasks of 100 mL BG-11 with Km, and incubated at 30
444 °C in 30 µmol photos· m^2· s^{-1} light for 1 day without shaking. The library culture was then
445 moved to 70 µmol photos· m^2· s^{-1} light on an orbital shaker till OD_{750} reached ~0.3. The
446 cultures were then combined, diluted to starting density of OD_{750} 0.025, and 4 replicates of 15
447 mL were spun down at 4,696 g and frozen at -80 °C as Time 0 samples to determine population
448 baseline. After transfering to bioreactors, CLC bioreactors were set for continuous light at 500
449 µmol photos· m^2· s^{-1} and LDC bioreactors were set to a square-wave cycle consisting of 12 h
450 light - 12 h dark. Bioreactors were set to run in turbidostat mode maintaining the density at
451 OD_{750} = 0.1. Bioreactors were sampled after approximately 6 generations: the CLC reactors
452 after 3 days (three 24-h light periods) and LDC reactors after 4 days (four 12-h light-12-h dark
453 light dark periods). Two of the three biological replicates for each condition were performed
454 concurrently (using 4 bioreactors) while a third was performed later using the same procedure
455 and conditions.

456 ***Bioluminescence monitoring***. Flask-grown batch cultures that reached a density of OD_{750} =
457 0.3-0.4 were diluted as needed to OD_{750} of 0.3 and 20 µL of each culture was placed on a pad
458 of BG-11 agar containing 10 µL of 100 mM firefly luciferin, in a well of a 96-well dish. Plates
459 were covered with clear tape to prevent drying and holes were poked using a sterile needle to
460 allow air transfer. Cultures were synchronized by incubating the plate under permissive LDC
461 conditions (0 and 30 µmol photos· m^2· s^{-1} light) for 3 days, and then returned to constant light
462 (LL) conditions for bioluminescence sampling by a Packard TopCount luminometer
463 (PerkinElmer Life Sciences). Bioluminescence of P_{kaiBC}*::luc* firefly luciferase fusion reporter was
464 monitored at 30 °C under CLC as described previously (54). Data were analyzed with the
465 Biological Rhythms Analysis Software System (http://millar.bio.ed.ac.uk/pebrown/
466 brass/brasspage.htm) import and analysis program using Microsoft Excel. Results shown are
467 the average of four biological replicate wells located in the innermost section of the plate, where
468 drying is minimal.

469 ***Protein sample preparation and gel electrophoresis, and Phos-tag acrylamide gels.***
470 Protein was isolated from cells and diluted to final loading concentration of 5 µg/well for RpaA
471 analysis and 10 µg/well for KaiC analysis (55). SDS/PAGE was performed according to
472 standard methods with the following exceptions. Phosphorylation of RpaA was detected using
473 10% SDS-polyacrylamide gels supplemented with Phos-tag ligand (Wako Chemicals USA) at a
474 final concentration of 25 µM and manganese chloride at a final concentration of 50 µM. Gels

were incubated once for 10 min in transfer buffer supplemented with 100 mM EDTA, followed by a 10-min incubation in transfer buffer without EDTA before standard wet transfer. Protein extracts and the electrophoretic apparatus were chilled to minimize hydrolysis of heat-labile phospho-Asp. Protein extracts for use in Phos-tag gels were prepared in Tris-buffered saline, and extracts for standard SDS/PAGE were prepared in PBS. RpaA antiserum (a gift from E. O'Shea, Harvard University, Cambridge, MA) was used at a dilution of 1:2,000 and secondary antibody (goat anti-rabbit IgG, Calbiochem Cat # 401315) at 1:5000. KaiC immunoblotting was performed similarly using KaiC antiserum diluted to 1:2000 and secondary antibody diluted to 1:10,000 (Horseradish Peroxidase-labeled goat anti-chicken IgY, Aves Labs, Cat # H-1004) (56). Densitometric analyses were performed using National Institutes of Health ImageJ software (52) (**Fig. S3, Dataset S3**). Samples were immediately stored at -80 °C, thawed once, and always kept on ice.

Fitness calculations

Of the 2,723 genes comprising the genome of *S. elongatus* 718 are essential, and mutants in the essential genes are not present in the library (24). To estimate the fitness effects of gene disruptions in LDC relative to CLC, we developed an analysis pipeline of curating the data from the 2,005 nonessential genes, normalizing it, and then analyzing it using linear models (**Dataset S1**). We first counted the number of reads for each sample to use as a normalizing factor between samples. Bar codes are dispersed across the genome, and we removed any bar code falling outside of a gene (24,868 bar codes out of 154,949 total bar codes) or within a gene but not within the middle 80% (27,763/154,949). Based on the bar codes remaining, we removed any gene not represented by at least three bar codes in different positions (114 genes out of 2,075 total). This filtering left us with 102,136 bar codes distributed across 1,961 genes.

For each bar code in each sample we added a pseudocount of one to the number of reads, divided by the total number of reads for the sample as calculated before, and took the log-2 transformation of this sample-normalized number of reads. The experiment involved two different starting pools of strains (called T0), each of which was divided into CLC and LDC samples. To account for different starting percentages of each bar code within the T0 pools, we averaged the log-2 transformed values for a bar code across the four replicate T0 samples for each pool then subtracted these average starting bar-code values from the CLC and LDC values in the respective pools. We also removed any gene without at least 15 T0 reads (across the four replicates and before adding the pseudocount) in each pool (89/1,961), leaving 1,872 genes and 101,258 bar codes.

For each gene, we used maximum likelihood to fit a pair of nested linear mixed effects models to the sample- and read-normalized log-2 transformed counts:

$$(1)\quad y_{i,j,k} = \mu_g + C_j + B_i + \varepsilon_{i,j,k}\ ;\ B_i \sim iid\ N(0,\varsigma_g^2)\ ;\ \varepsilon_{i,j,k} \sim iid\ N(0,\sigma_g^2)$$

$$(2)\quad y_{i,j,k} = \mu_g + B_i + \varepsilon_{i,j,k}\ ;\ B_i \sim iid\ N(0,\varsigma_g^2)\ ;\ \varepsilon_{i,j,k} \sim iid\ N(0,\sigma_g^2)$$

where $y_{i,j,k}$ is the normalized log-2 value for bar code i in gene g in condition j for sample k, μ_g is the average value for the gene, C_j is the fixed effect of condition j, B_i is a random effect for bar code i, and $\varepsilon_{i,j,k}$ is the residual. We identified genes with significant fitness differences between conditions by comparing the difference in the -2*log likelihoods of the models to a chi-square distribution with one degree of freedom, estimating a p-value, accounting for multiple testing by the false-discovery rate method of Benjamini and Hochberg (57), and selecting those gene with

521 adjusted p-values less than 0.01. We took the contrast $C_{LDC} - C_{CLC}$ to be the estimated LDC-
522 specific fitness effect of knocking out the gene (**Dataset S2**).

523 Results obtained across biological replicates and across similar screens performed in either
524 batch cultures grown in 250 mL Erlenmeyer shake flasks and on solid agar on Petri plates were
525 consistent **(Fig. S4, Dataset S4**). Mutants that had estimated fitness scores below a confidence
526 threshold (associated FDR adjusted p-value <0.01) (**Dataset S2**) were not considered. Mutants
527 with gene disruptions that had an LDC fitness score ≥ 1.0 or ≤ -1.0 with a false discovery rate ≤
528 1% were classified having strong fitness phenotype specific to growth in LDC, and those with a
529 fitness score of < 1.0 but ≥ 0.5 and > -1.0 but ≤ -0.5 were classified as causing a moderate
530 fitness phenotype. Fitness scores <0.5 and >-0.5 were categorized as negligent/minor, i.e., little
531 change in abundance over the course of the experiment in LDC vs. CLC.

532 ***Fluorescence Spectroscopy.*** To monitor the formation of the CikA activating complex,
533 fluorescence anisotropy measurements were performed at 30 °C on an ISS PC1
534 spectrofluorometer equipped with a three-cuvette sample compartment, at excitation and
535 emission wavelengths of 492 nm and 530 nm, respectively, for samples including 6-
536 iodoacetamidofluorescein (6-IAF) labeled KaiB-FLAG-K251C alone (0.05 μM), and its mixtures
537 with KaiC (4 μM) or FLAG-CikA (4 μM) or KaiC (4 μM) + FLAG-CikA (4 μM). Each sample (400
538 μL) was either in an ATP buffer [20 mM Tris, 150 mM NaCl, 5 mM $MgCl_2$, 1 mM ATP, 0.5 mM
539 EDTA, 0.25 mM TCEP (tris(2-carboxyethyl)phosphine), pH 8.0] or in ATP/ADP buffer [20 mM
540 Tris, 150 mM NaCl, 5 mM $MgCl_2$, 0.5 mM ATP, 0.5 mM ADP, 0.5 mM EDTA, 0.25 mM TCEP,
541 pH 8.0]. TCEP was introduced from the FLAG-CikA stock [20 mM Tris, 150 mM NaCl, 5 mM
542 TCEP, pH 8.0]. KaiB stock was in the buffer [20 mM Tris, 150 mM NaCl, pH 8.0] and KaiC stock
543 in the buffer [20 mM Tris, 150 mM NaCl, 5 mM $MgCl_2$, 1 mM ATP, 0.5 mM EDTA, pH 8.0].

544 The KaiC samples included freshly dephosphorylated WT KaiC, and KaiC phosphomimetics
545 KaiC-AE and KaiC-EA. To prepare the freshly dephosphorylated KaiC, WT KaiC at 20 μM in the
546 buffer [20 mM Tris, 150 mM NaCl, 5 mM $MgCl_2$, 1 mM ATP, 0.5 mM EDTA, pH 8.0] was
547 incubated at 30 °C for 24 hours before the fluorescence binding assays. SDS-PAGE analysis
548 was performed to determine KaiC and CikA stability and KaiC phosphorylation levels (**Fig. S5**,
549 **Dataset S5**).

550

551 ## Acknowledgments

552 This work was supported by research grants (R35GM118290 to SSG; R01GM107521 to AL) and
553 training grants (T32GM007240 to BER and SD) from the National Institutes of Health and the
554 National Science Foundation (MCB1517482 to SAR).

555

556 ## References

557 1. Ouyang Y, Andersson CR, Kondo T, Golden SS, Johnson CH (1998) Resonating circadian
558 clocks enhance fitness in cyanobacteria. *Proc Natl Acad Sci U S A* 95(15):8660–8664.

559 2. Woelfle MA, Ouyang Y, Phanvijhitsiri K, Johnson CH (2004) The adaptive value of
560 circadian clocks: an experimental assessment in cyanobacteria. *Curr Biol* 14(16):1481–
561 1486.

562 3. Lambert G, Chew J, Rust MJ (2016) Costs of Clock-Environment Misalignment in Individual
563 Cyanobacterial Cells. *Biophys J* 111(4):883–891.

564 4. Yerushalmi S, Yakir E, Green RM (2011) Circadian clocks and adaptation in *Arabidopsis*.
565 *Mol Ecol* 20(6):1155–1165.

566 5. Dodd AN, et al. (2005) Plant circadian clocks increase photosynthesis, growth, survival,
567 and competitive advantage. *Science* 309(5734):630–633.

568 6. Morris CJ, Yang JN, Scheer FAJL (2012) The impact of the circadian timing system on
569 cardiovascular and metabolic function. *Prog Brain Res* 199:337–358.

570 7. Kelleher FC, Rao A, Maguire A (2014) Circadian molecular clocks and cancer. *Cancer Lett*
571 342(1):9–18.

572 8. Kim JH, Duffy JF (2018) Circadian Rhythm Sleep-Wake Disorders in Older Adults. *Sleep*
573 *Med Clin* 13(1):39–50.

574 9. Chaix A, Zarrinpar A, Panda S (2016) The circadian coordination of cell biology. *J Cell Biol*
575 215(1):15–25.

576 10. Nakajima M, et al. (2005) Reconstitution of circadian oscillation of cyanobacterial KaiC
577 phosphorylation in vitro. *Science* 308(5720):414–415.

578 11. Tseng R, et al. (2017) Structural basis of the day-night transition in a bacterial circadian
579 clock. *Science* 355(6330):1174–1180.

580 12. Paddock ML, Boyd JS, Adin DM, Golden SS (2013) Active output state of the
581 *Synechococcus* Kai circadian oscillator. *Proc Natl Acad Sci U S A* 110(40):E3849–57.

582 13. Gutu A, O'Shea EK (2013) Two antagonistic clock-regulated histidine kinases time the
583 activation of circadian gene expression. *Mol Cell* 50(2):288–294.

584 14. Markson JS, Piechura JR, Puszynska AM, O'Shea EK (2013) Circadian control of global
585 gene expression by the cyanobacterial master regulator RpaA. *Cell* 155(6):1396–1408.

586 15. Diamond S, et al. (2017) Redox crisis underlies conditional light-dark lethality in
587 cyanobacterial mutants that lack the circadian regulator, RpaA. *Proc Natl Acad Sci U S A*
588 114(4):E580–E589.

589 16. Puszynska AM, O'Shea EK (2017) Switching of metabolic programs in response to light
590 availability is an essential function of the cyanobacterial circadian output pathway. *Elife* 6.
591 doi:10.7554/eLife.23210.

592 17. Swan JA, Golden S, LiWang A, Partch CL (2018) Structure, function, and mechanism of the
593 core circadian clock in cyanobacteria. *J Biol Chem*. doi:10.1074/jbc.TM117.001433.

594 18. Iwasaki H, et al. (2000) A *kaiC*-interacting sensory histidine kinase, SasA, necessary to
595 sustain robust circadian oscillation in cyanobacteria. *Cell* 101(2):223–233.

596 19. Boyd JS, Bordowitz JR, Bree AC, Golden SS (2013) An allele of the crm gene blocks
597 cyanobacterial circadian rhythms. *Proc Natl Acad Sci U S A* 110(34):13950–13955.

598 20. Diamond S, Jun D, Rubin BE, Golden SS (2015) The circadian oscillator in *Synechococcus*
599 *elongatus* controls metabolite partitioning during diurnal growth. *Proc Natl Acad Sci U S A*
600 112(15):E1916–25.

601 21. Gründel M, Scheunemann R, Lockau W, Zilliges Y (2012) Impaired glycogen synthesis
602 causes metabolic overflow reactions and affects stress responses in the cyanobacterium
603 *Synechocystis* sp. PCC 6803. *Microbiology* 158(Pt 12):3032–3043.

604 22. Puszynska AM, O'Shea EK (2017) ppGpp Controls Global Gene Expression in Light and in
605 Darkness in *S. elongatus*. *Cell Rep* 21(11):3155–3165.

606 23. Hood RD, Higgins SA, Flamholz A, Nichols RJ, Savage DF (2016) The stringent response
607 regulates adaptation to darkness in the cyanobacterium *Synechococcus elongatus*. *Proc*
608 *Natl Acad Sci U S A* 113(33):E4867–76.

609 24. Rubin BE, et al. (2015) The essential gene set of a photosynthetic organism. *Proc Natl*
610 *Acad Sci U S A* 112(48):E6634–43.

611 25. Broddrick JT, et al. (2016) Unique attributes of cyanobacterial metabolism revealed by
612 improved genome-scale metabolic modeling and essential gene analysis. *Proc Natl Acad*
613 *Sci U S A* 113(51):E8344–E8353.

614 26. Wetmore KM, et al. (2015) Rapid quantification of mutant fitness in diverse bacteria by
615 sequencing randomly bar-coded transposons. *MBio* 6(3):e00306–15.

616 27. Vijayan V, Zuzow R, O'Shea EK (2009) Oscillations in supercoiling drive circadian gene
617 expression in cyanobacteria. *Proc Natl Acad Sci U S A* 106(52):22564–22568.

618 28. Miao X, Wu Q, Wu G, Zhao N (2003) Changes in photosynthesis and pigmentation in an
619 agp deletion mutant of the cyanobacterium *Synechocystis* sp. *Biotechnol Lett* 25(5):391–
620 396.

621 29. Li X, Shen CR, Liao JC (2014) Isobutanol production as an alternative metabolic sink to
622 rescue the growth deficiency of the glycogen mutant of *Synechococcus elongatus* PCC
623 7942. *Photosynth Res* 120(3):301–310.

624 30. Porankiewicz J, Clarke AK (1997) Induction of the heat shock protein ClpB affects cold
625 acclimation in the cyanobacterium *Synechococcus* sp. strain PCC 7942. *J Bacteriol*
626 179(16):5111–5117.

627 31. Gill RT, et al. (2002) Genome-wide dynamic transcriptional profiling of the light-to-dark
628 transition in *Synechocystis* sp. strain PCC 6803. *J Bacteriol* 184(13):3671–3681.

629 32. Hagemann M, Vinnemeier J, Oberpichler I, Boldt R, Bauwe H (2005) The glycine

630 decarboxylase complex is not essential for the cyanobacterium *Synechocystis* sp. strain
631 PCC 6803. *Plant Biol* 7(1):15–22.

632 33. Hackenberg C, et al. (2009) Photorespiratory 2-phosphoglycolate metabolism and
633 photoreduction of O2 cooperate in high-light acclimation of *Synechocystis* sp. strain PCC
634 6803. *Planta* 230(4):625–637.

635 34. Cohen SE, Golden SS (2015) Circadian Rhythms in Cyanobacteria. *Microbiol Mol Biol Rev*
636 79(4):373–385.

637 35. Ishiura M, et al. (1998) Expression of a gene cluster *kaiABC* as a circadian feedback
638 process in cyanobacteria. *Science* 281(5382):1519–1523.

639 36. Nishiwaki T, et al. (2004) Role of KaiC phosphorylation in the circadian clock system of
640 *Synechococcus elongatus* PCC 7942. *Proc Natl Acad Sci U S A* 101(38):13927–13932.

641 37. Xu Y, et al. (2004) Identification of key phosphorylation sites in the circadian clock protein
642 KaiC by crystallographic and mutagenetic analyses. *Proc Natl Acad Sci U S A*
643 101(38):13933–13938.

644 38. Williams SB, Vakonakis I, Golden SS, LiWang AC (2002) Structure and function from the
645 circadian clock protein KaiA of *Synechococcus* elongatus: a potential clock input
646 mechanism. *Proc Natl Acad Sci U S A* 99(24):15357–15362.

647 39. Ditty JL, Canales SR, Anderson BE, Williams SB, Golden SS (2005) Stability of the
648 *Synechococcus elongatus* PCC 7942 circadian clock under directed anti-phase expression
649 of the kai genes. *Microbiology* 151(Pt 8):2605–2613.

650 40. Nair U, Ditty JL, Min H, Golden SS (2002) Roles for sigma factors in global circadian
651 regulation of the cyanobacterial genome. *J Bacteriol* 184(13):3530–3538.

652 41. Schmitz O, Katayama M, Williams SB, Kondo T, Golden SS (2000) CikA, a
653 bacteriophytochrome that resets the cyanobacterial circadian clock. *Science*
654 289(5480):765–768.

655 42. Chen Y, et al. (2009) A novel allele of *kaiA* shortens the circadian period and strengthens
656 interaction of oscillator components in the cyanobacterium *Synechococcus elongatus* PCC
657 7942. *J Bacteriol* 191(13):4392–4400.

658 43. Kutsuna S, Nakahira Y, Katayama M, Ishiura M, Kondo T (2005) Transcriptional regulation
659 of the circadian clock operon kaiBC by upstream regions in cyanobacteria. *Mol Microbiol*
660 57(5):1474–1484.

661 44. Chang Y-G, et al. (2015) Circadian rhythms. A protein fold switch joins the circadian
662 oscillator to clock output in cyanobacteria. *Science* 349(6245):324–328.

663 45. Kitayama Y, Iwasaki H, Nishiwaki T, Kondo T (2003) KaiB functions as an attenuator of
664 KaiC phosphorylation in the cyanobacterial circadian clock system. *EMBO J* 22(9):2127–
665 2134.

666 46. Rust MJ, Golden SS, O'Shea EK (2011) Light-driven changes in energy metabolism directly
667 entrain the cyanobacterial circadian oscillator. *Science* 331(6014):220–223.

47. Ito H, et al. (2009) Cyanobacterial daily life with Kai-based circadian and diurnal genome-wide transcriptional control in *Synechococcus elongatus*. *Proc Natl Acad Sci U S A* 106(33):14168–14173.

48. Matson MM, Atsumi S (2017) Photomixotrophic chemical production in cyanobacteria. *Curr Opin Biotechnol* 50:65–71.

49. McEwen JT, Kanno M, Atsumi S (2016) 2,3 Butanediol production in an obligate photoautotrophic cyanobacterium in dark conditions via diverse sugar consumption. *Metab Eng* 36:28–36.

50. Snijder J, et al. (2017) Structures of the cyanobacterial circadian oscillator frozen in a fully assembled state. *Science* 355(6330):1181–1184.

51. Taton A, et al. (2014) Broad-host-range vector system for synthetic biology and biotechnology in cyanobacteria. *Nucleic Acids Res* 42(17):e136.

52. Schneider CA, Rasband WS, Eliceiri KW (2012) NIH Image to ImageJ: 25 years of image analysis. *Nat Methods* 9(7):671–675.

53. Clerico EM, Ditty JL, Golden SS (2007) Specialized techniques for site-directed mutagenesis in cyanobacteria. *Methods Mol Biol* 362:155–171.

54. Mackey SR, Golden SS, Ditty JL (2011) The itty-bitty time machine genetics of the cyanobacterial circadian clock. *Adv Genet* 74:13–53.

55. Ivleva NB, Golden SS (2007) Protein extraction, fractionation, and purification from cyanobacteria. *Methods Mol Biol* 362:365–373.

56. Dong G, et al. (2010) Elevated ATPase activity of KaiC applies a circadian checkpoint on cell division in *Synechococcus elongatus*. *Cell* 140(4):529–539.

57. Benjamini Y, Hochberg Y (1995) Controlling the False Discovery Rate: A Practical and Powerful Approach to Multiple Testing. *J R Stat Soc Series B Stat Methodol* 57(1):289–300.

58. Ditty JL, Williams SB, Golden SS (2003) A cyanobacterial circadian timing mechanism. *Annu Rev Genet* 37:513–543.

Figure Legends

Fig 1. Using RB-TnSeq to assess genetic contributions to fitness in LDC. A dense pooled mutant library containing unique known bar-code identification sequences linked to each individual gene insertion was used to estimate the fitness of each loss-of-function mutant grown under alternating light-dark conditions. The library was grown under continuous light and sampled to determine the baseline abundance of each strain in the population prior to transfer to photobioreactors which were then either exposed to continuous light or alternating 12-h light - 12-h dark regimes. Bar-code quantification of the library population in both conditions was normalized to the baseline and compared against each other to estimate the fitness consequences of loss of function of each gene specific to growth in LDC.

Fig 2. LDC Rb-TnSeq screen results breakdown. *(A)* Of the 2723 genes in the genome, 1872 genes were analyzed in the library population. Of those, data from mutants with loss-of-function of 1420 genes fell below our false discovery threshold. Of the remaining 452 genes, 220 had moderate to strong fitness effects. ***(****B)* A volcano plot highlighting genes of interest. Red-shaded region indicates an estimated fitness decrease in LDC and the green-shaded region indicates a fitness increase. ***(****C)* Functional category composition of genes that gave strong fitness scores. Categories based on COG classification or GO ID. Green corresponds to strong fitness increases; Red corresponds to strong fitness decreases.

Fig. 3. Connection between essential night-time metabolism and RpaA regulation. *(A)* A metabolic map showing the reactions (red) that are controlled by genes that are essential in LDC. Reactions that are non-essential (solid arrows) or essential (dashed arrows) in CLC are are also indicated. Stars mark NADPH-generating reactions. * gene was not revealed in the screen but is known to be required in LDC; # minor LDC decrease measured, likely due to fitness contribution in CLC which affects calculation **(***B****)*** LDC-sensitive mutant population enriched for genes known to be positively regulated by RpaA.

Fig. 4. *kaiA* mutant growth and *cikA*-based intervention in LDC. *(A)* Dilution spot-plate growth of strains in CLC and LDC. A representation of the genotype of each strain is portrayed next to each dilution series. Shaded grey bar at end of *kaiA* = negative regulatory element. *(B)* *cikA* mutant fitness increase in competition with WT in LDC and CLC. *(C)* Growth of liquid cultures in replicate photobioreactors in LDC. Vertical shaded areas represent dark conditions. Shaded areas around each line = standard deviation of biological replicates.

Fig. 5. Bioluminescence levels from *kaiBC* reporter in mutant backgrounds. The intensity of P_{kaiBC}*::luc* output signal correlates with LDC sensitivity. Rhythms were measured in CLC conditions driven by the *kaiBC* promoter after exposure to 72 h of entraining LDC that includes a low-light intensity that is permissive for the mutants. Shaded areas around each line = standard deviation of biological replicates.

Fig. 6. RpaA status correlates with growth success in LDC. *(A)* RpaA phosphorylation at dusk (after 12 h light) showing average ± SD values. Letters indicate groupings from ANOVA analysis. ***(****B)* Levels of KaiC from cells taken at dusk. **C.** RpaA phosphorylation across the light-dark transitions beginning with dawn. ***(****D)* H_2DCFDA fluorescence over a 12-h dark period during an LDC, indicating total cellular ROS in WT, $kaiA^{del}$, and $kaiA^{del}cikA$. The shaded area indicates the period of darkness following a 12-h light period. P-RpaA denotes phosphorylated protein.

740 **Fig. 7. CikA-activating complex formation.** *(A)* Fluorescence anisotropy of the binding
741 kinetics of 6-IAF–labeled KaiB (black) to WT KaiC, KaiA-AE, or KaiC-EA (red in each case) with
742 and without CikA (blue), and in the presence of 0.5 mM ATP + 0.5 mM ADP. ***(B)*** Binding of KaiB
743 (black) to WT KaiC or KaiC-AE (red in each case) with and without CikA (blue) in the presence
744 of 1.0 mM ATP.

745 **Fig. 8. Model for LDC sensitivity due to circadian clock disfunction.** ***(A)*** Conventionally, the
746 role of KaiA is primarily to bind to the A-loops of the CII domain of KaiC, stimulating its
747 autophosphorylation and consequently increasing the activity of the kinase SasA; this activity in
748 turn results in accumulation of phosphorylated RpaA throughout the day. P-RpaA initiates the
749 expression of circadian-controlled night-time class 1 genes at dusk. ***(B)*** Without KaiA, KaiC
750 phosphorylation is suppressed and, thus, SasA kinase activity is diminished, reducing the pools
751 of SasA-mediated P-RpaA. Upon KaiC-KaiB complex formation, CikA has access to binding
752 sites usually occupied by KaiA, and becomes hyperactive; excessive CikA phosphatase activity
753 extinguishes intracellular pools of P-RpaA and eliminates the cell's ability to express essential
754 genes needed for survival in LDC. Figure modified from (11). The dotted line in thepanel B
755 graph represents the WT levels of P-RpaA from A.

756

757 ## Supplemental Material

758 ## Dataset Files

759 **Dataset S1**: This zipped file contains the annotated R script for determining genetic fitness
760 estimates under LDC and the data files processed by the script: 1)
761 "lightdarkbioreactors_all.poolcount.csv.", the location and reads of bar-coded transposon
762 mutants for each sample 2) "lightdarkbioreactors_exp.csv", designation of the samples as T0,
763 control genotype, and experimental genotype 3) "genes.tab", the gene coordinate file used to
764 map bar-coded transposon mutants to genes.

765 **Dataset S2**: This Excel file has the following tabs: 1) Fitness estimates determined by
766 processing the files in Dataset S1. 2) Search utility for displaying information easily for a desired
767 gene locus id.

768 **Dataset S3**: This Excel table contains two sheets: 1) The data calculated from the Phos-tag™
769 immunoblots for RpaA phosphorylation and the corresponding blots they were derived from in
770 Fig. S3; and 2) Data in a format for entering into R and using the script provided in the text box
771 to perform the statistical analysis that generated the groupings in Fig. 6A.

772 **Dataset S4**: RB-TnSeq data comparing photobioreactor biological replicates, and the estimates
773 from analysis of the library grown in triplicate in photobioreactors with the library grown on Petri
774 plates and in 100 mL shake flasks under similar LDC conditions.

775 **Dataset S5**: This Excel file contains the data from the anisotropy measurements of *in vitro* KaiB,
776 KaiC, and CikA.

777

778

779 **Supplemental Table**

780 **Table S1**

Strain	Genetic background	Reporter	Antibiotic resistance	Reference
AMC541	WT *S.elongatus*	P_{kaiBC} *: : luc*;	Cm	(42)
AMC06	WT *S.elongatus*	none	none	Lab collection
AMC1161	*kaiA* insertion; pAM2969 in AMC541	P_{kaiBC} *: : luc*;	Cm Km	(58)
AMC702	*kaiA* deletion; in-frame markerless constructed in AMC541	P_{kaiBC} *: : luc*;	Cm	(58)
AMC1936	*kaiABC* knockout; pAM4252 in AMC541	P_{kaiBC} *: : luc*;	Cm Km	(12)
AMC1679	*kaiA cikA* double knockout; pAM2152 in AMC702	P_{kaiBC} *: : luc*;	Cm Gm	(56)
AMC2479	Complemented *kaiA cikA* double knockout; pAM3389 expressing *cikA* in AMC1679	P_{kaiBC} *: : luc*;	Cm SpSm	This study
AMC1100	Complemented *kaiA* deletion; pAM2246 in AMC702 expressing WT *kaiA* in NS1.	P_{kaiBC} *: : luc*;	Cm SpSm	(39)
AMC2480	Complemented *kaiA cikA* double knockout AMC1679 with pAM5294 expressing $cikA^{C644R}$ variant.	P_{kaiBC} *: : luc*;	Cm SpSm	This study
AMC2481	*kaiA* deletion; pAM5389 in AMC541	P_{kaiBC} *: : luc*;	Cm SpSm	This study
AMC2482	Remade *kaiA cikA* double knockout; pAM2152 in AMC2481	P_{kaiBC} *: : luc*;	Cm SpSm Gm	This study
AMC2483	Remade *kaiA cikA* double knockout; pAM2152 in AMC702	P_{kaiBC} *: : luc*;	Cm Gm	This study

781

782

783 **Fig. S1. Mutant strain complementation reverses phenotype.** *(A)* Dilution spot plate showing
784 growth of various *kaiA* mutant strains under CLC or LDC conditions. Reintroduction of *kaiA*
785 greatly improves the growth of the *kaiA* deletion mutant (compare rows 6 and 3 in LDC);
786 reintroduction of *cikA* into the *kaiA*^{del}*cikA* double mutant reverses the alleviating effects of *cikA*
787 disruption (compare rows 7 and 4) ***(B)*** Genetic map showing a representation of the strain
788 backgrounds. **C.** DNA gel electrophoresis of PCR amplification confirming mutations in *kaiA*
789 gene in *kaiA* mutant strains.

790 **Fig. S2. Effect of antibiotic marker expression during head-to-head growth competition.**
791 WT cultures with antibiotic resistance cassettes for either Gm or Km in a neutral site of the
792 genome were mixed in a 1:1 ratio and competed against each other in a head-to-head growth
793 assay without antibiotics under CLC and LDC conditions.

794 **Fig. S3. Immunoblots for determining RpaA phosphorylation and KaiC levels.** For blots A-
795 F Phos-tag™ was added to cell extracts to distinguish phosphorylated from non-phosphorylated
796 proteins and antisera were used to identify the labeled protein in each panel. Panels A-B and G
797 show proteins taken from cells sampled at the end of the light period after 3 consecutive 12-h
798 light:12-h dark cycles. Panels E-F show samples taken every 12 h over the course of a 12-h
799 light: 12-h dark cycle; even lanes are samples at the end of the dark period and odd lanes are
800 samples taken at the end of the light period. Genotypes of strains are listed in Table S1.

801 *(A)* lanes: 1, AMC541; 2, AMC702; 3, AMC2481; 4, AMC2481; 5, AMC2482; 6, AMC2482; 7,
802 AMC1679; 8, AMC2480; 9, AMC2480; 10, AMC2479; 11, AMC2479; 12, AMC2483; 13,
803 AMC1161; 14, AMC1936;

804 *(B)* lanes: 1, AMC541; 2, AMC1161; 3, AMC702; 4, AMC1936; 5, AMC1679; 6, AMC2479.

805 *(C)* lanes: 1, AMC541; 2, AMC1161; 3, AMC702; 4, AMC1679; 5, AMC1100; 6, AMC2479; 7,
806 empty; 8, AMC541; 9, AMC2481; 10, AMC702; 11, empty; 12, AMC1936; 13, empty.

807 *(D)* lanes: 1-6, AMC541; 7-12, AMC702.

808 *(E)* lanes: 1-6, AMC541; 7-12, AMC702.

809 *(F)* lanes 1-6, AMC541; 7-12, AMC1679.

810 *(G)* lanes: 1, AMC541; 2, AMC1161; 3, AMC2481; 4, AMC2482; 5, empty; 6, AMC2482; 7,
811 empty; 8, AMC541; 9, AMC1161; 10, AMC702; 11, AMC1679; 12, AMC1936.

812 **Fig. S4. Comparison of LDC Rb-TnSeq results across replicates and growth conditions.**
813 *(A)* Strain fitness for each photobioreactor replicate was estimated as previously described in
814 (24)**.** Fitness scores with t-statistics ≥ |4| were compared against each other showing agreement
815 among biological replicates. *(B)* Comparison of LDC fitness results screening the library in
816 different growth formats including photobioreactors, Erlenmeyer flasks, and Petri plates.
817 Because there was only 1 measurement each for the plates and flask screens, the stringency
818 for sensitivity scores was relaxed. *(C)* Summary of the 13 mutant strains that showed strong
819 LDC defects across all growth media situations.

820 **Fig. S5. SDS-PAGE analysis of KaiC and CikA stability and KaiC dephosphorylation.** *(A)*
821 17% SDS-PAGE analysis of KaiC-EA or KaiC-AE and CikA before and after KaiB binding
822 assays. *(B)* 17% SDS-PAGE analysis of KaiC and CikA stability before and after KaiB binding
823 assays. *(C)* 6.5% SDS-PAGE analysis showing that KaiC retains a hypophosphorylated state
824 during KaiB-binding assays. Note that all samples other than the controls contain 6-IAF-labeled
825 KaiB-FLAG-K25C. Due to the low concentration of KaiB (0.05 μM), SDS-PAGE runs were
826 optimized only for visualization of KaiC and CikA. The stable anisotropy readings of free KaiB,
827 shown in Fig. 7, suggest its stability for the duration of the binding assays.

828 **Figure 1**

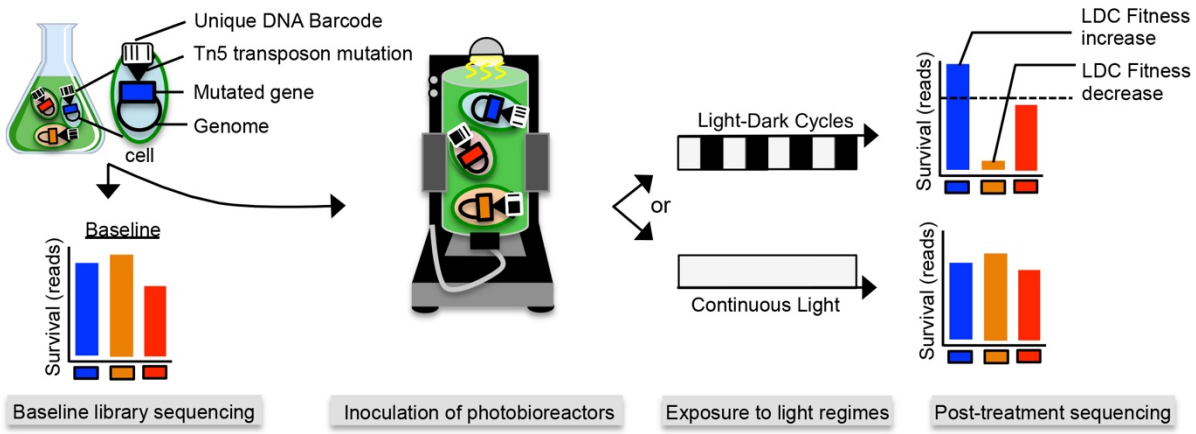

829

830 **Figure 2**

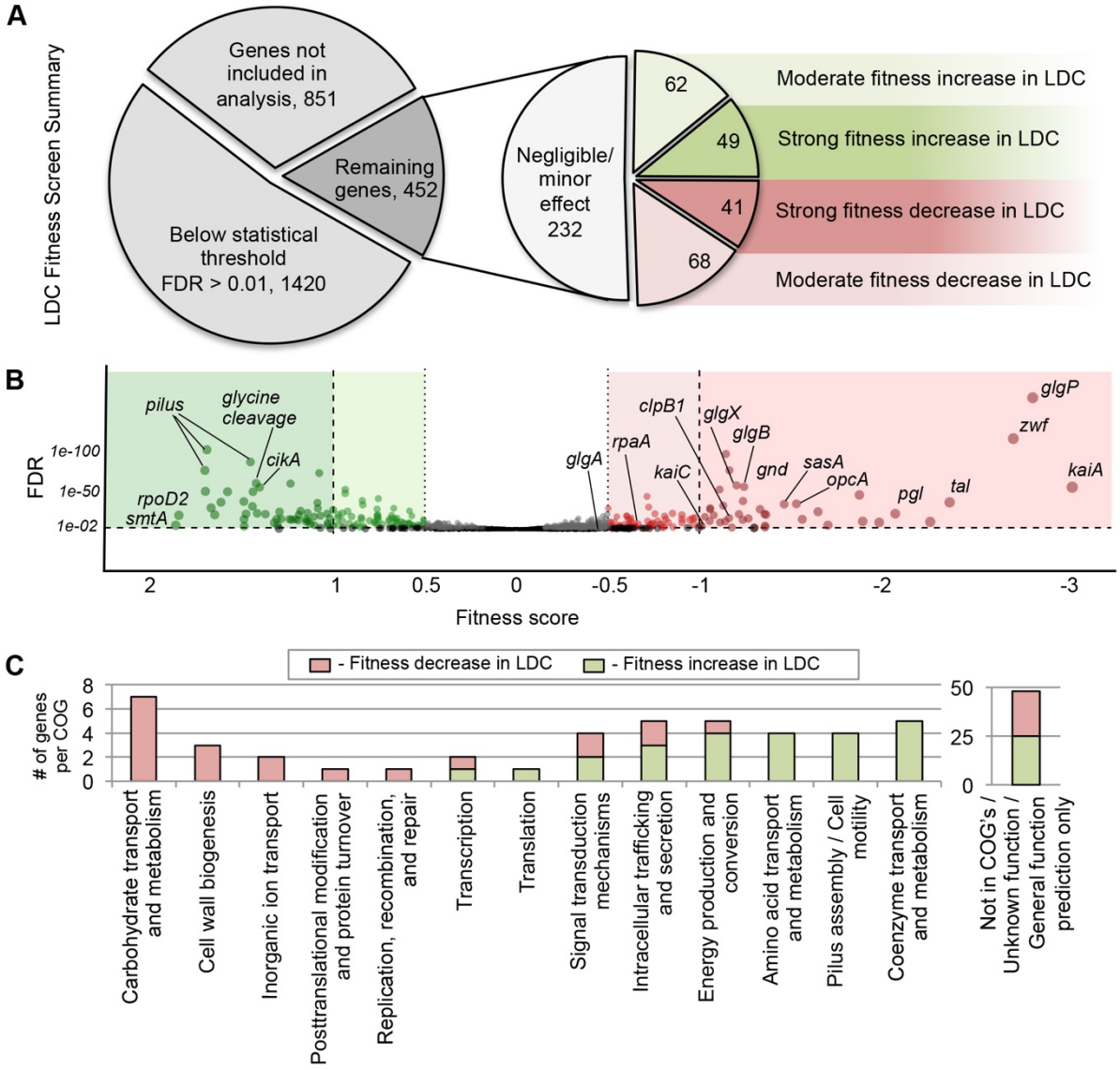

831

832 **Figure 3**

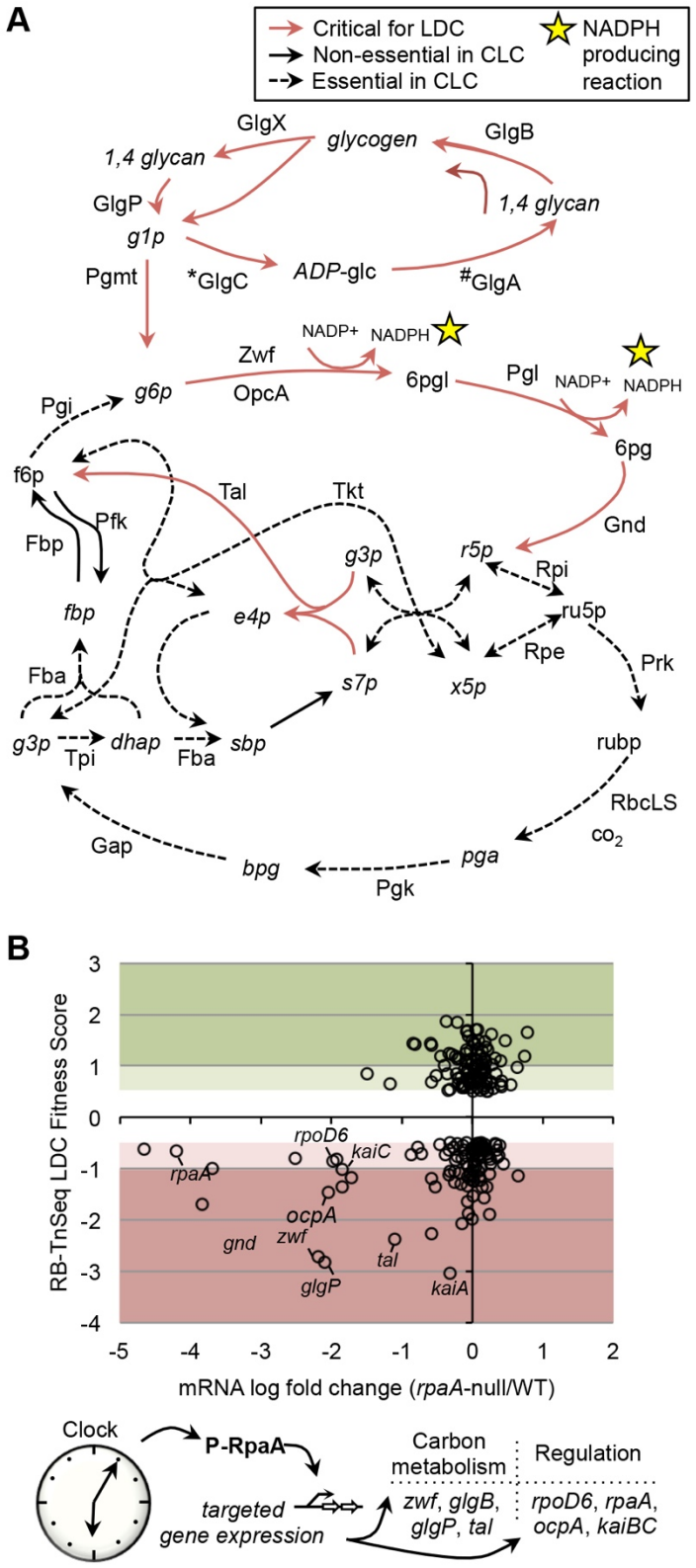

833

834

835 **Figure 4**

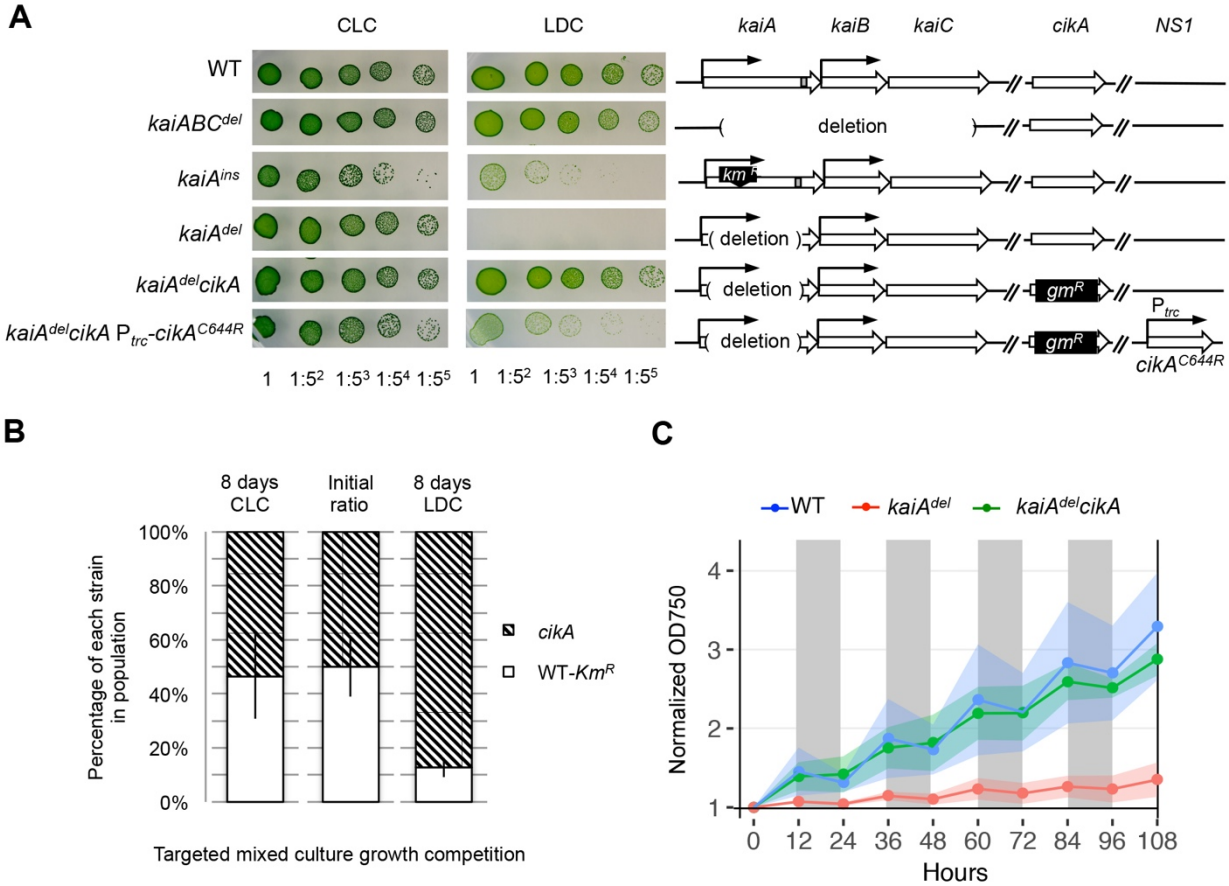

836

837 **Figure 5**

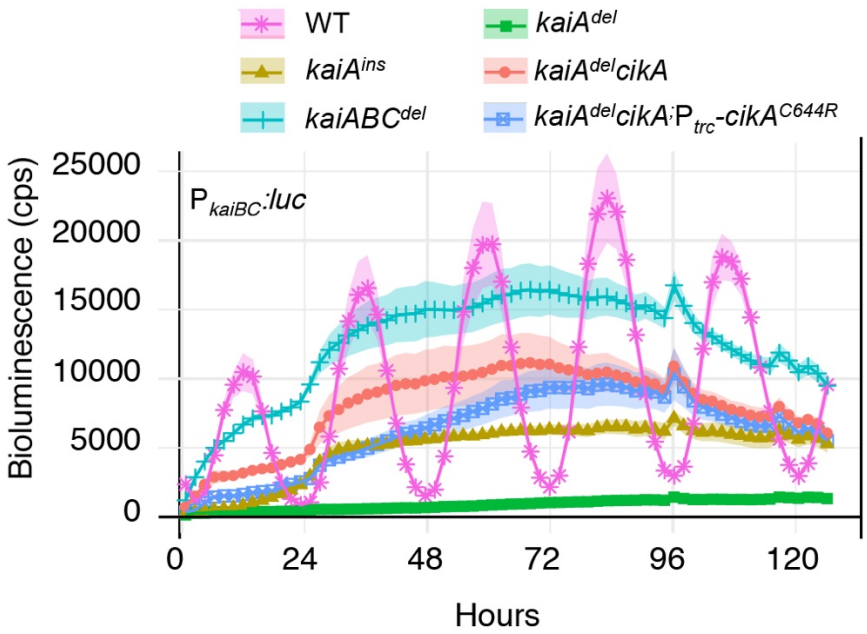

838

839 **Figure 6**

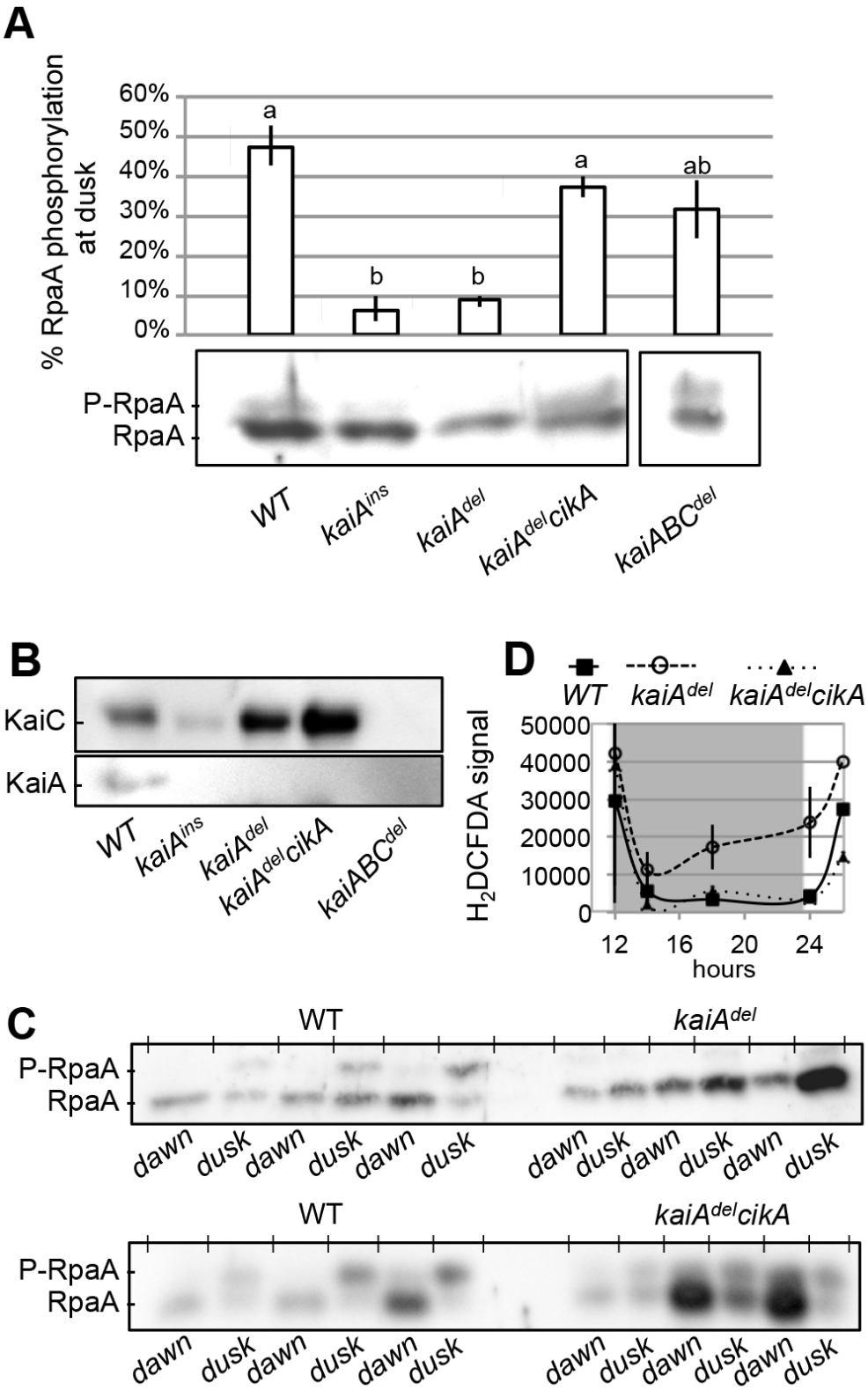

840

841

842 **Figure 7**

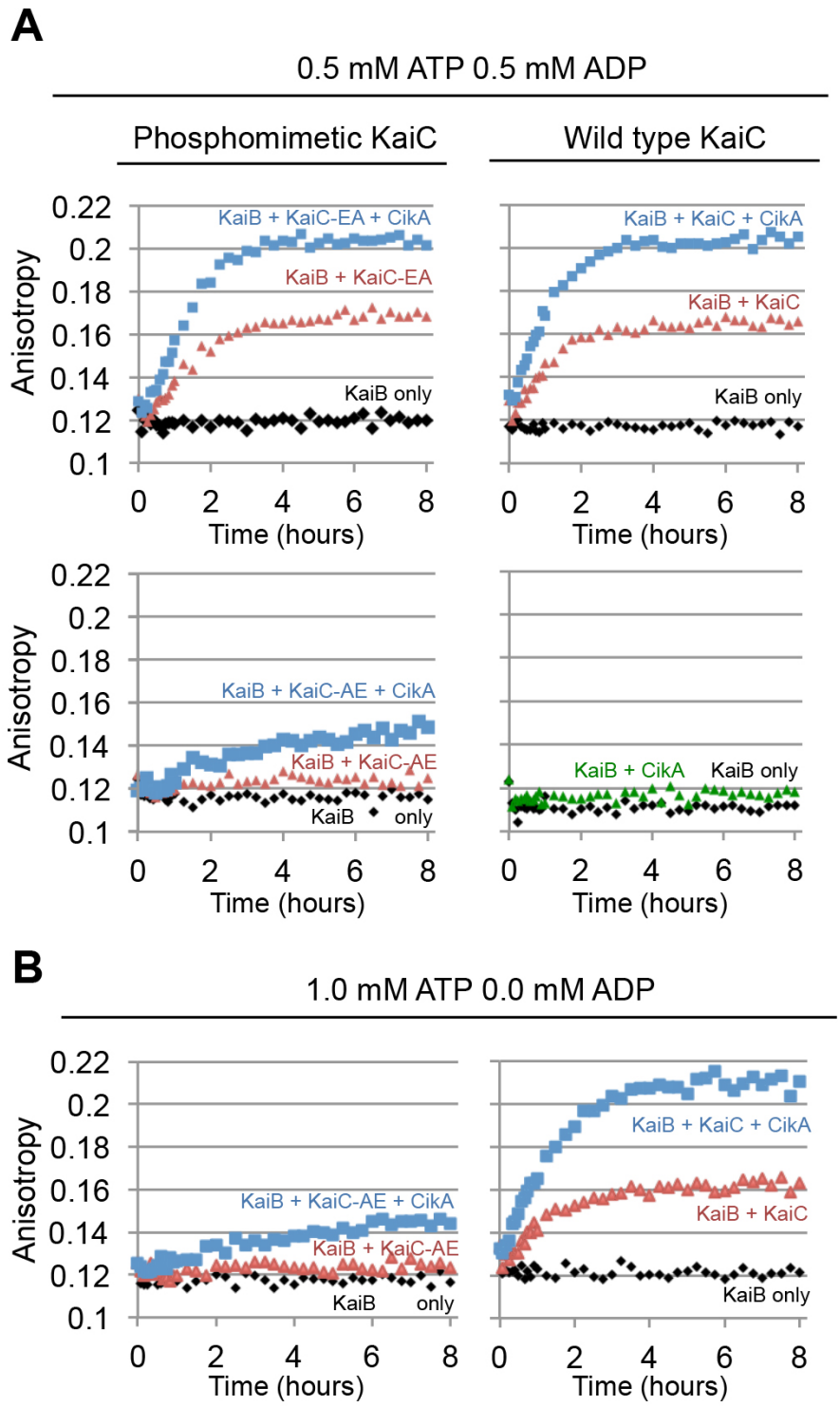

843

844 **Figure 8**

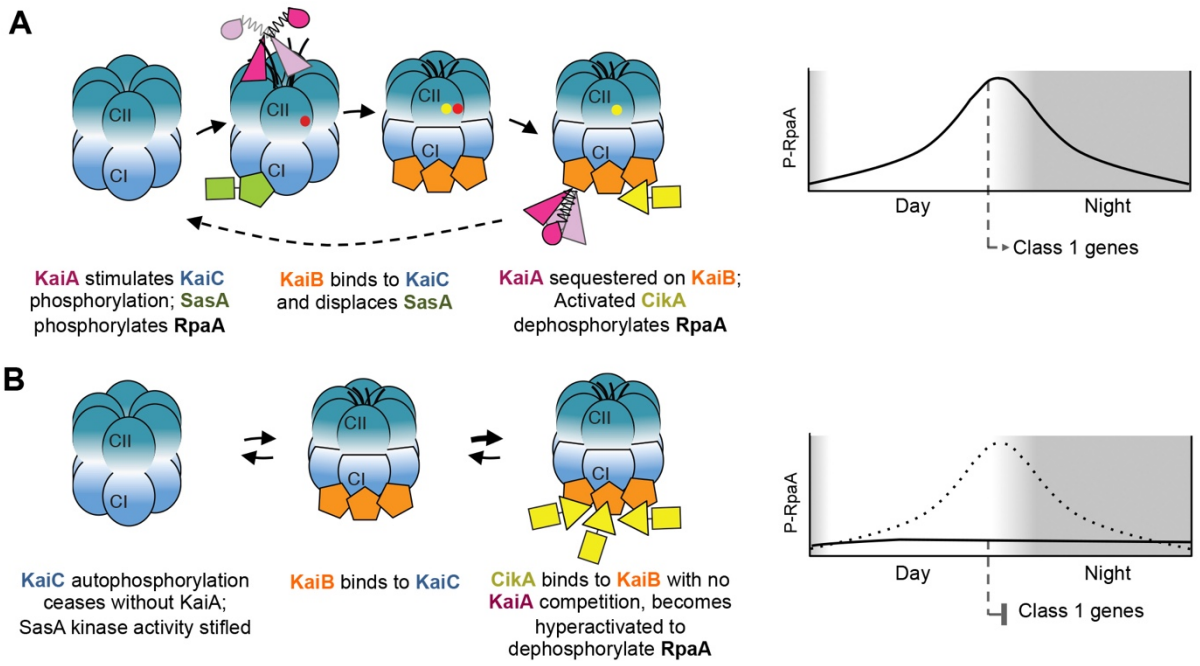

845

846 **Figure S1**

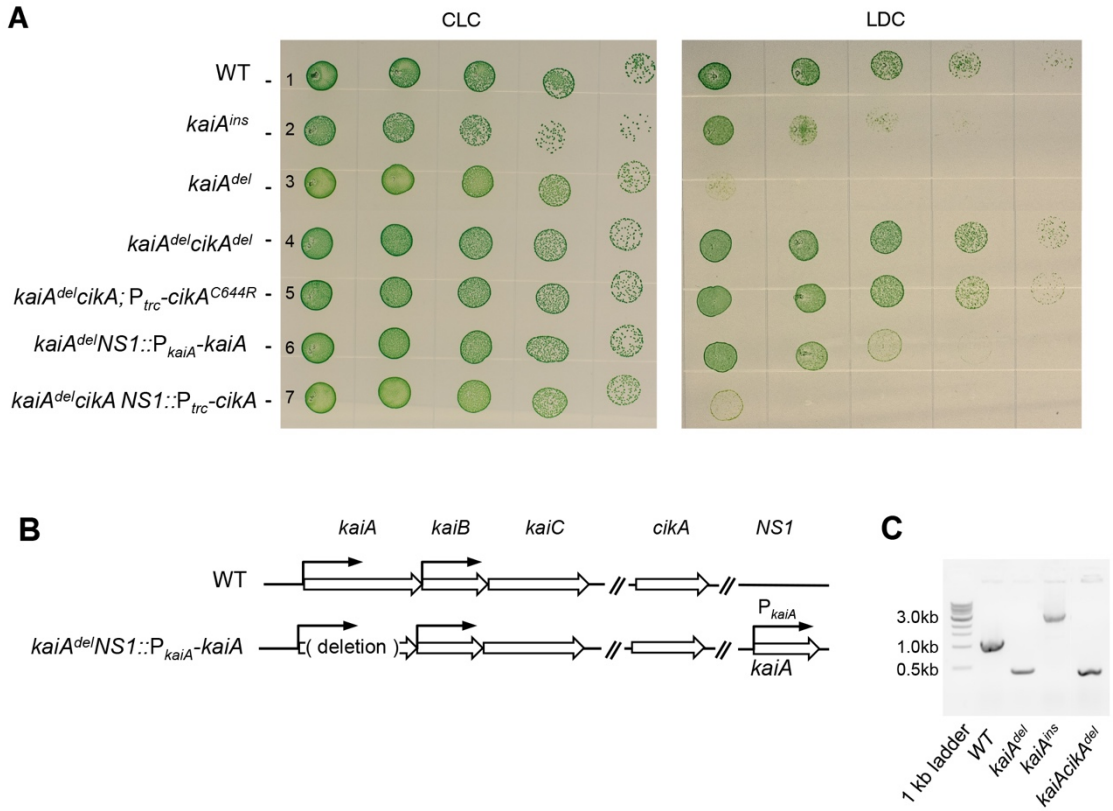

847

848 **Figure S2**

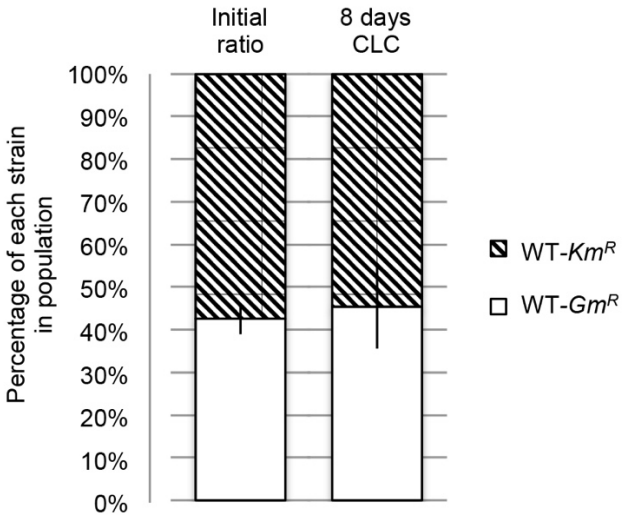

849

850 **Figure S3**

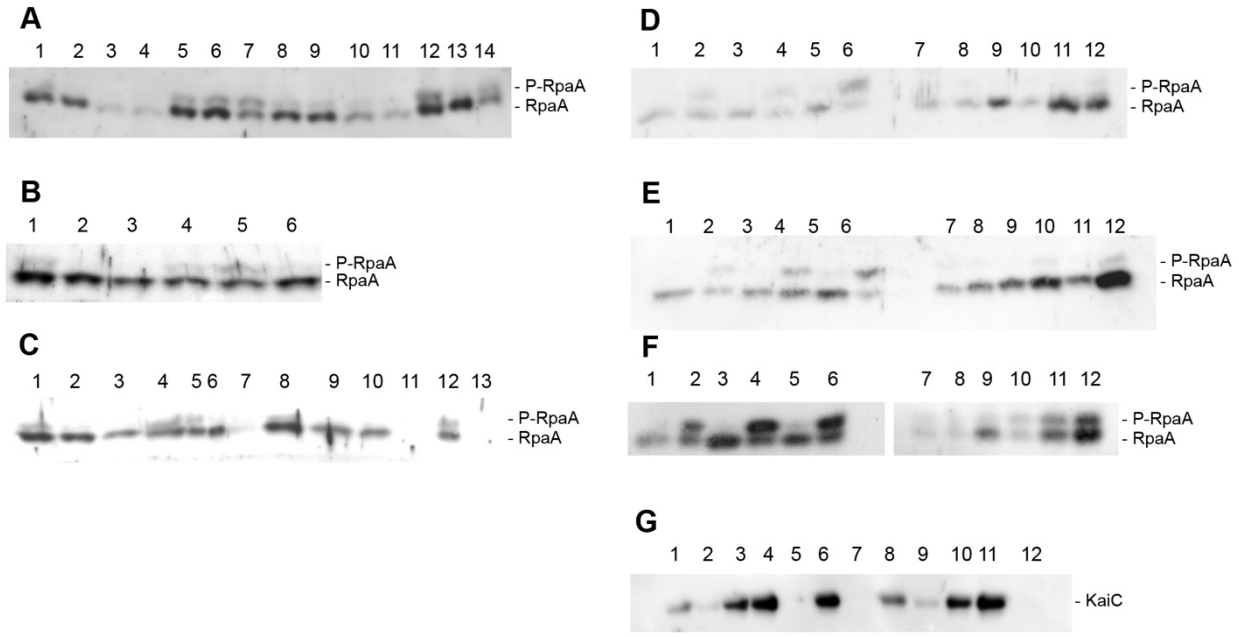

851

852 **Figure S4**

A

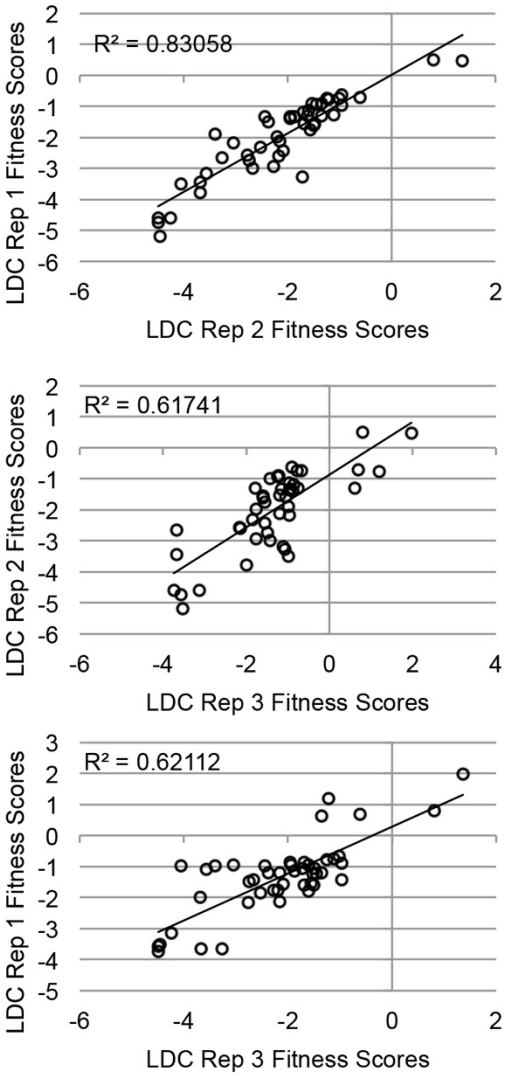

B

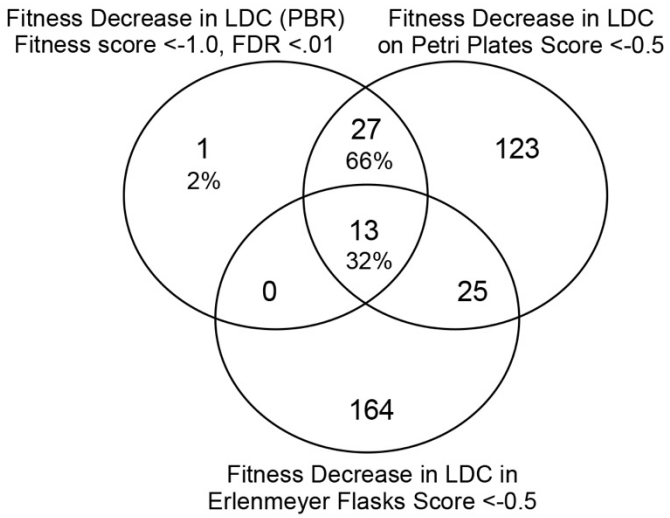

C

locusId	Description	Flask	Plate	PBR
0039	6-phosphogluconate dehydrogenase	-3.4	-3.2	-1.4
2334	glucose-6-phosphate 1-dehydrogenase	-3.6	-3.2	-2.7
1218	circadian clock protein KaiA	-3.5	-2.5	-3.0
2114	sensory kinase SasA	-2.4	-2.4	-1.5
0518	hypothetical protein	-1.1	-2.1	-1.4
2297	transaldolase	-2.7	-1.4	-2.4
0347	hypothetical protein	-2.3	-1.4	-1.3
1216	circadian clock protein KaiC	-1.9	-1.1	-1.0
0156	phosphoglucomutase	-0.9	-3.8	-1.1
1417	hypothetical protein	-0.8	-1.2	-1.3
0529	6-phosphogluconolactonase	-0.8	-1.0	-2.1
0244	glycogen phosphorylase	-3.7	-0.8	-2.8
2076	ribosome-associated GTPase	-0.9	-0.6	-1.1

853

854 **Figure S5**

SDS-PAGE analysis of KaiC and CikA stability and KaiC dephosphorylation:
(A) 17% SDS-PAGE analysis of KaiC-EA or KaiC-AE and CikA; (B) 17% SDS-PAGE analysis of KaiC and CikA;
(C): 6.5 % SDS-PAGE gels showing that KaiC remained hypophosphorylated during KaiB binding assays

A

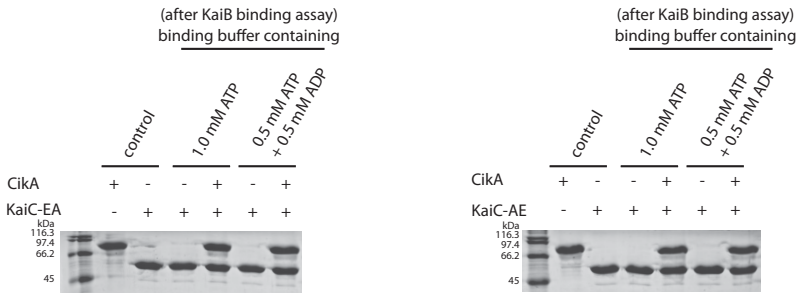

B

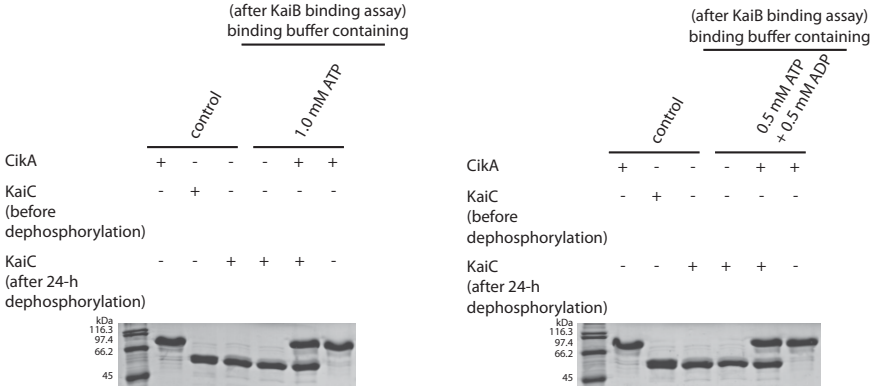

C

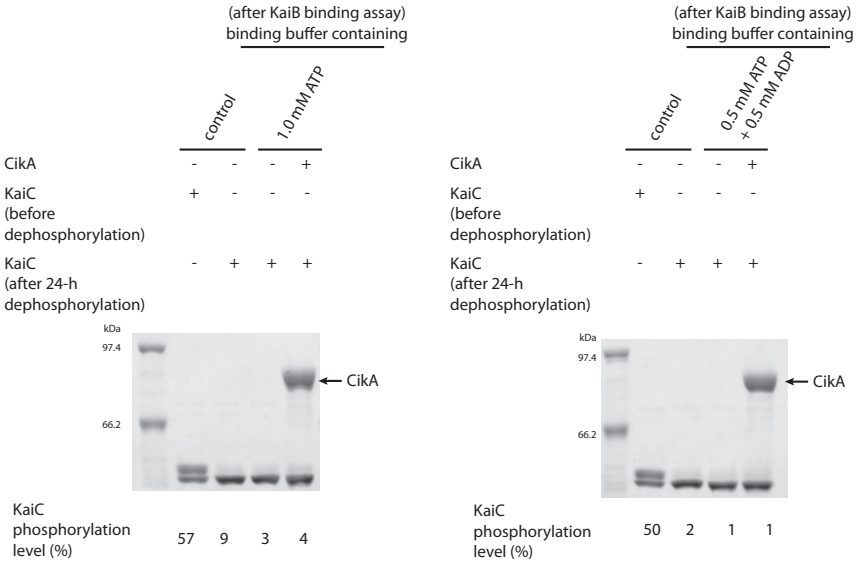

855